

Discriminating Superimposed Alteration Associated with Epigenetic Base and Precious Metal Vein Systems in the Rouyn-Noranda Mining District, Quebec; Implications for Exploration in Ancient Volcanic Districts

Marina D. Schofield,^{1,†} Bruno Lafrance,¹ Harold L. Gibson,¹ K. Howard Poulsen,² Christophe Scheffer,³ Benoît Quesnel,³ Georges Beaudoin,³ and Michael A. Hamilton⁴

¹Metal Earth, Mineral Exploration Research Center, Harquail School of Earth Sciences, Laurentian University, 935 Ramsey Lake Road, Sudbury, Ontario P3E 2C6, Canada

²Consultant, 34 Wallford Way, Ottawa, Ontario K2E 6B6, Canada

³Département de géologie et de génie géologique, Centre E4m, Université Laval, Quebec, Quebec G1V 0A6, Canada ⁴Jack Satterly Geochronology Laboratory, University of Toronto, 22 Ursula Franklin Street, Toronto, Ontario M5S 3B1, Canada

Abstract

The Rouyn-Noranda mining district of Quebec contains 20 Cu-Zn (±Au ±Ag) volcanogenic massive sulfide (VMS) deposits, including the giant and gold-rich Quemont and Horne deposits. Mineralized epigenetic veins are also present, but their origin and relative timing remain enigmatic. The nature and extent of their alteration signatures and the effect of their superposition on district-scale alteration patterns is unknown. The VMSrelated quartz-sulfide Cu-Zn-Ag veins have $\delta^{18}O_{quartz}$ values of 8.5 \pm 0.8‰, reflecting $\delta^{18}O_{fluid}$ compositions of -0.4 to 3.1% (250°-350°C) that are typical of Archean seawater. They are associated with a proximal Fe-rich chlorite alteration and marginal spotted sericite-chlorite alteration with whole-rock δ^{18} O values of 2.9 to 5.9% and are interpreted to have formed within the structurally controlled discordant upflow zones of a VMS hydrothermal system. Younger gold-bearing quartz-carbonate veins were emplaced along mechanical anisotropies created by mafic dikes during north-south compression and the formation of regional E-trending faults, folds, and cleavage. They are characterized by $\delta^{18}O_{quartz}$ values of 11.3 \pm 0.8%, reflecting $\delta^{18}O_{fluid}$ compositions of 2.4 to 5.9% (250°-350°C), typical of a metamorphic fluid, possibly mixed with a lower δ^{18} O upper crustal fluid. They are associated with ankerite, calcite, muscovite, chlorite, albite, and quartz ± hematite alteration with whole-rock δ^{18} O values of 5.8 to 10.3‰. Chemical abrasion-isotope dilution-thermal ionization mass spectrometry (CA-ID-TIMS) U-Pb zircon ages for two tonalite intrusions constrain the maximum age of the Cu-Zn-Ag veins to 2697.6 ± 0.7 Ma and the minimum age to 2695.3 ± 1.0 Ma, which is also the maximum age of the gold quartz-carbonate veins. Superposition of alteration related to the gold quartz-carbonate veins on previously chlorite- and sericite-altered rocks has resulted in mixed alteration signals with whole-rock δ^{18} O values of ~6 to 8‰ that have perturbed and masked regional alteration patterns related to older VMS mineralization, such as those found in the Quemont and Horne deposits. These results indicate that defining alteration vectors in camps that have superimposed hydrothermal systems requires full consideration of the hydrothermal history of the camp, and if such constraints are lacking, whole-rock δ^{18} O values should not be used as a stand-alone exploration method.

Introduction

Quartz-sulfide(-oxide) veins associated with phyllosilicate mineral alteration assemblages are ubiquitous to virtually all hydrothermal ore deposits (e.g., porphyry, epithermal, volcanogenic massive sulfide [VMS], and orogenic gold) regardless of age or tectonic setting. The internal textures of these veins are typically nonunique, and where they are overprinted by subsequent deformation events, early vein types (e.g., porphyry, epithermal, VMS) may be similar to later orogenic veins (Robert and Poulsen, 2001). Further complexity arises when multiple deposit types are superposed within a district—a common feature of modern evolving orogens (Sillitoe, 1978; Sawkins, 1990; Blundell, 2002) and greenstone belts (Hutchinson, 1987; Dubé and Mercier-Langevin, 2020; Tripp et al., 2020). For example, three superposed mineralization types have been documented at the Archean Boddington deposit in the Yilgarn craton, Western Australia: early porphyry-style quartz-

sulfide Cu (±Au) vein mineralization, intrusion-related Au-Cu-Mo-Bi mineralization, and younger orogenic Au mineralization (Turner et al., 2020). Likewise, the origin of the Cu-Au veins of the Archean Chapais-Chibougamau mining camp in the Abitibi greenstone belt in Canada has long been debated as either syntectonic or magmatic-hydrothermal (Watkins and Riverin, 1982; Guha et al., 1983; Pilote et al., 1995; Leclerc et al., 2012; Dubé and Mercier-Langevin, 2020). These veins are hosted by brittle-ductile shear zones that are associated with tonalite and quartz-diorite dike swarms and quartz, carbonate, sericite, and chlorite alteration assemblages. They are now interpreted as magmatic-hydrothermal in origin, with the shear zones superposed during later deformation and associated locally with orogenic gold mineralization (Dubé and Mercier-Langevin, 2020). In complex environments with superimposed hydrothermal systems it is essential to decipher the tectonic and magmatic events because this knowledge impacts our understanding of deposit formation and paleohydrothermal and tectonomagmatic processes, which also have implications for exploration models and strategies.

†Corresponding author: e-mail, mschofield@laurentian.ca

Recognition of superimposed mineralization and its effects have been largely overlooked in the Rouyn-Noranda mining district of Quebec (Fig. 1), which contains 20 VMS deposits, 19 orogenic gold quartz-carbonate vein deposits, and several enigmatic breccia-hosted and vein-style Cu-Zn-Ag prospects, occurrences, and deposits (Gibson and Galley, 2007). The Cu-Zn-Ag quartz-sulfide veins have been interpreted as synvolcanic and related to VMS mineralization (Gibson et al., 1983; Zubowski, 2011), as epigenetic and related to Cu-(Mo) intrusion-related deposits (Kirkham, 1972; Kotila, 1975; Goldie et al., 1979; Kennedy, 1985; Jebrak et al., 1997; Galley and van Breemen, 2002), or as epigenetic but younger than the gold quartz-carbonate veins (McMurchy, 1948). The timing of the gold quartz-carbonate vein deposits is also uncertain and controversial and has been interpreted as syntectonic (Riverin et al., 1990; Robert et al., 1996) or posttectonic (Mc-Murchy, 1948; Carrier et al., 2000) relative to the main period of north-south shortening across the district. Moreover, the relative timing and alteration footprints of the superposed Cu-Zn-Ag quartz and gold quartz-carbonate veins have also not been documented.

In this paper we use field work, geochronology, and mineral and isotope geochemistry of vein and alteration assemblages in the Rouyn-Noranda mining district to (1) demonstrate the relative chronology of the two vein types with respect to each other and regional structural fabrics, (2) present new interpretations for their emplacement and origin, (3) characterize and contrast their alteration and oxygen isotope signatures, and (4) evaluate the effects of their superimposed alteration on mineralogical, geochemical, and isotopic alteration vectors used for VMS and gold exploration. We demonstrate at least three superposed mineralization events within the district and show the efficacy of these tools for determining the timing and origin of multigenerational veins in ancient volcanic districts. Moreover, we illustrate the potential pitfalls of using alteration vectors defined from whole-rock oxygen isotope data in districts that have superposed hydrothermal events.

Regional Geology of the Rouyn-Noranda Mining District

Rouyn-Noranda is a gold and base metal mining district within the 2704 to 2695 Ma Blake River Group in the

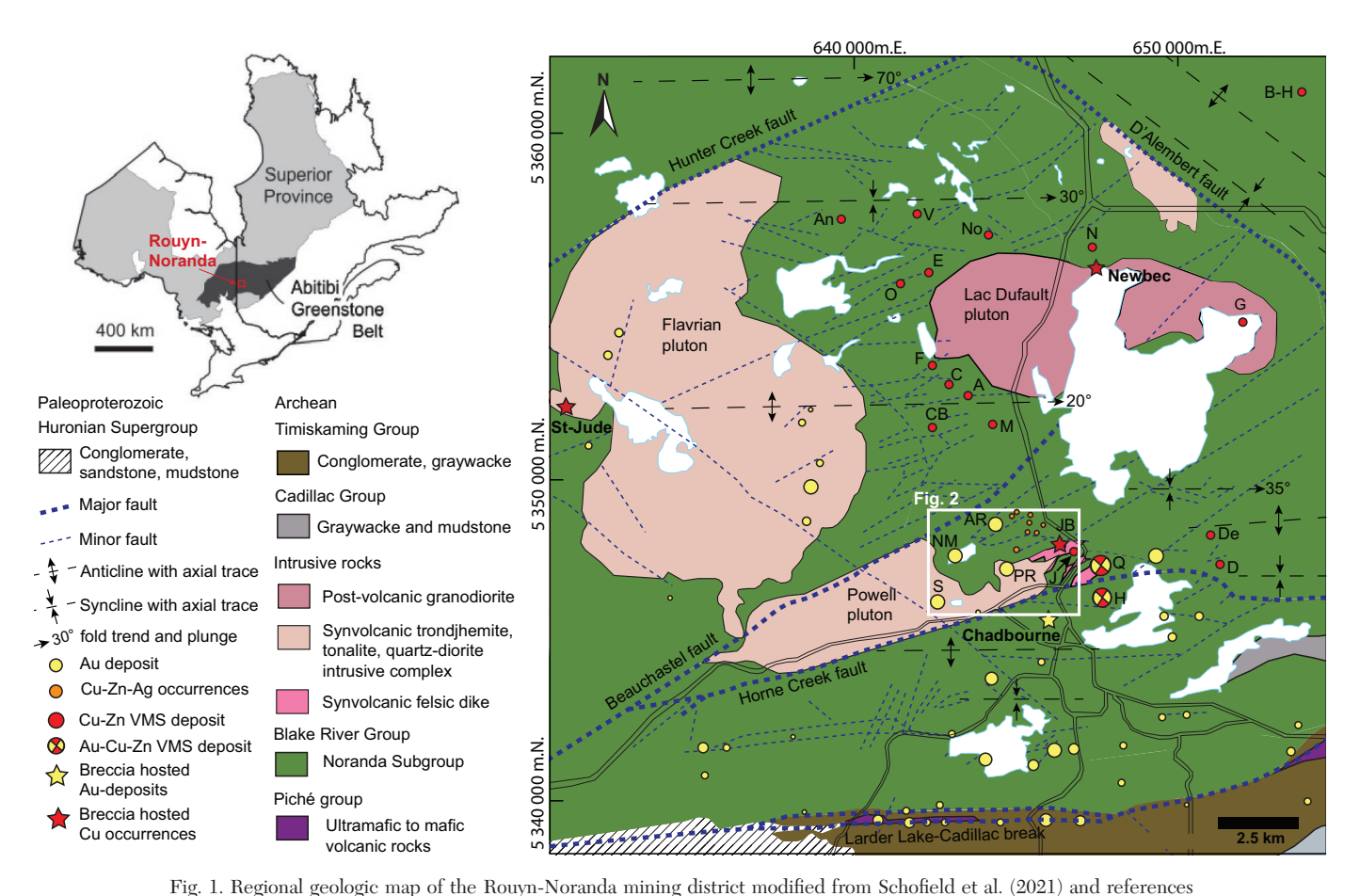


Fig. 1. Regional geologic map of the Rouyil-Noranda mining district modified from Scholieid et al. (2021) and references therein, showing spatial distribution of the various mineral occurrences and deposits. Anticlines and synclines shown are F₂ structures, major and minor faults are unsubdivided. The yellow circles are scaled to reflect the relative gold tonnage. Abbreviations for volcanogenic massive sulfide (VMS) deposits: A = Amulet A, An = Ansil, B-H = Bouchard-Hebert, C = Amulet C, CB = Corbet, D = Delbridge, De = Deldona, E = East Waite, F = Amulet F, G = Gallen, H = Horne, J = Joliet, M = Millenbach, N = Newbec, No = Norbec, O = Old Waite, Q = Quemont, V = Vauze. Abbreviations for other deposits: AR = Anglo-Rouyn, DR = Don Rouyn, JB = Joliet breccia, NM = New Marlon, PR = Powell Rouyn, S = Silidor. Location for Figure 2 is highlighted by the white rectangle.

Abitibi subprovince of the Archean Superior province (Fig. 1). It is centered on a 6-km-thick bimodal volcanic package of the Noranda volcanic complex, which is interpreted to have formed as a submarine shield volcano with a diameter of 40 to 50 km (De Rosen Spence, 1976). Volcanic strata and their massive sulfide deposits are subdivided into older (2703–2701 Ma) and younger (2699–2695 Ma) Blake River Group, separated by a brief hiatus in volcanism at ~2700 Ma (McNicoll et al., 2014). The VMS deposits are localized along NE- and NW-striking synvolcanic structures (Scott, 1980; Knuckey and Watkins, 1982; Knuckey et al., 1982; Setterfield et al., 1995), and the Flavrian and Powell intrusive complexes along the western margin of the district have been interpreted as the synvolcanic heat source that drove hydrothermal circulation and the formation of some of the VMS deposits within the district (Gibson and Galley, 2007).

The Noranda volcanic complex is located ~5 km north of the Larder Lake Cadillac Break, a major E-W-striking belt-scale structure (Fig. 1) associated with alluvial-fluvial successions of polymictic conglomeratic rocks, cross-bedded sandstone, and alkali-shoshonitic volcanic rocks of the Timiskaming Group and numerous orogenic gold deposits (Poulsen, 2017; Dubé and Mercier-Langevin, 2020). The district has experienced at least three deformational events. A pre-Timiskaming deformation event produced E-W- to NW-trending F₁ folds, which lacks an axial planar cleavage, and is expressed by an angular unconformity between the folded and tilted ca. 2704 to 2695 Ma Blake River Group metavolcanic rocks and the ca. 2676 to 2669 Ma Timiskaming Group (Wilson, 1956; Poulsen, 2017). The main post-Timiskaming deformation in the district occurred between ca. 2670 to 2660 Ma, with the most intense strain in proximity to the Larder Lake Cadillac Break (Daigneault et al., 2002; Robert et al., 2005; Bedeaux et al., 2017; Dubé and Mercier-Langevin, 2020). Subsequently, NW-SE-directed shortening resulted in dextral transcurrent reactivation of the Larder Lake Cadillac and Porcupine Destor faults (Dimroth et al., 1983; Hubert et al., 1984; Wilkinson et al., 1999; Daigneault et al., 2002; Ispolatov et al., 2008; Bleeker, 2012; Bedeaux et al., 2017; Poulsen, 2017). The main post-Timiskaming folding event is referred to as D2 and the dextral transcurrent event is referred to as D₃ (Goulet, 1978; Dimroth et al., 1983; Hubert et al., 1984).

Gold deposits within the district are located along the Larder Lake Cadillac Break, along related second- and third-order structures (e.g., Horne Creek fault), or within competent intrusive bodies (e.g., Flavrian and Powell intrusive complexes). The timing of orogenic gold mineralization within the southern Abitibi greenstone belt remains controversial, but most authors suggest mineralization occurred during the main period of regional deformation, characterized by north-south shortening (e.g., Kerrich and Kyser, 1994; Bedeaux et al., 2017; Dubé and Mercier-Langevin, 2020) that coincided with ~2669 to 2653 Ma peak metamorphism in the southern Abitibi greenstone belt (Powell et al., 1995; Piette-Lauzière et al., 2019; Dubé and Mercier-Langevin, 2020).

Regional metamorphism of the Noranda district resulted in subgreenschist to greenschist facies assemblages (Powell et al., 1995) that are superimposed on older amphibolite facies assemblages that define a 2.5-km-wide contact metamorphic aureole around the postvolcanic, 2690.3 +2.2/–2.0 Ma

(Mortensen, 1993) Lac Dufault pluton. The aureole is defined by hornblende and biotite in unaltered volcanic rocks, and spotted cordierite, biotite, anthophyllite, and cummingtonite assemblages in hydrothermally altered volcanic rocks associated with VMS deposits (De Rosen-Spence, 1969; Hall, 1982; Fitchett, 2012). Pristine cordierite is rare and has retrograded to a fine-grained mineral association of sericite (muscovite and paragonite), quartz, biotite, and chlorite during later regional metamorphism (Walker, 1930; Cooke et al., 1931; Wilson, 1941; De Rosen-Spence, 1969; Fitchett, 2012). All rock types discussed in this study are metamorphosed, so the "meta" prefix has been omitted for brevity.

Methodology

Field mapping and sampling of both Cu-Zn-Ag quartz sulfide and gold quartz-carbonate veins were conducted at a scale of 1:100 using aerial drone images as base maps. Sampling transects were oriented perpendicular to the veins to determine the extent of their alteration footprints. Mineralized samples were analyzed for metal tenor and representative altered and least altered samples were analyzed for whole-rock compositions at ALS Geochemistry, Sudbury, Ontario. Results are included in Appendix Tables A1 and A2. Selected splits of the pulverized samples were also submitted for whole-rock δ^{18} O analysis (n = 85). Results are included in Appendix Table A3. In addition, representative samples of quartz (n = 11) from each of the veins were sent for $\delta^{18}O_{quartz}$ analysis at Laval University; results are included in Appendix Table A4. Mineralogical compositions were determined using the scanning electron microscope (SEM) and energy-dispersive spectroscopy (EDS) at the Mineral Exploration Research Centre Isotope Geochemistry Laboratory of Laurentian University. A TESCAN VEGA3 SEM was used with a beam intensity of 18 nA, at 15.00 kV, and a working distance of 15 mm. Results are included in Appendix Table A5. High-precision chemical abrasion-isotope dilution-thermal ionization mass spectrometry (CA-ID-TIMS) U-Pb zircon geochronology (Table 1) was completed at the Jack Satterly Geochronology Laboratory, University of Toronto. Full details on sample preparation and analytical techniques are included in Appendix A6.

Geology of the Powell Block

The Powell block is bound to the north by the Beauchastel fault and to the south by the Horne Creek fault and contains an abundance of these two enigmatic vein types within spatial proximity (Fig. 2). It comprises a bimodal transitional to calc-alkaline volcanic sequence of effusive mafic volcanic rocks, intercalated with lesser, localized aphyric and quartzphyric rhyolite flow dome complexes and minor volcaniclastic rocks. The strata have an overall north-northwest strike and moderate-to-steep east-northeast dip of 70° to 80° but are offset along NE- to ENE-striking faults and folded into E-W-trending, moderately E-plunging anticlines and synclines (Fig. 1, 3). To the west, the volcanic strata are intruded by the subvolcanic Powell intrusive complex, which comprises sill-like bodies of quartz diorite and younger tonalite and trondjhemite (Goldie, 1976). The age of the volcanic package within the study area is constrained to ca. 2702 to 2700 Ma (McNicoll et al., 2014; Schofield et al., 2021) but a younger ca. 2698 Ma magmatic event is locally superposed on the vol-

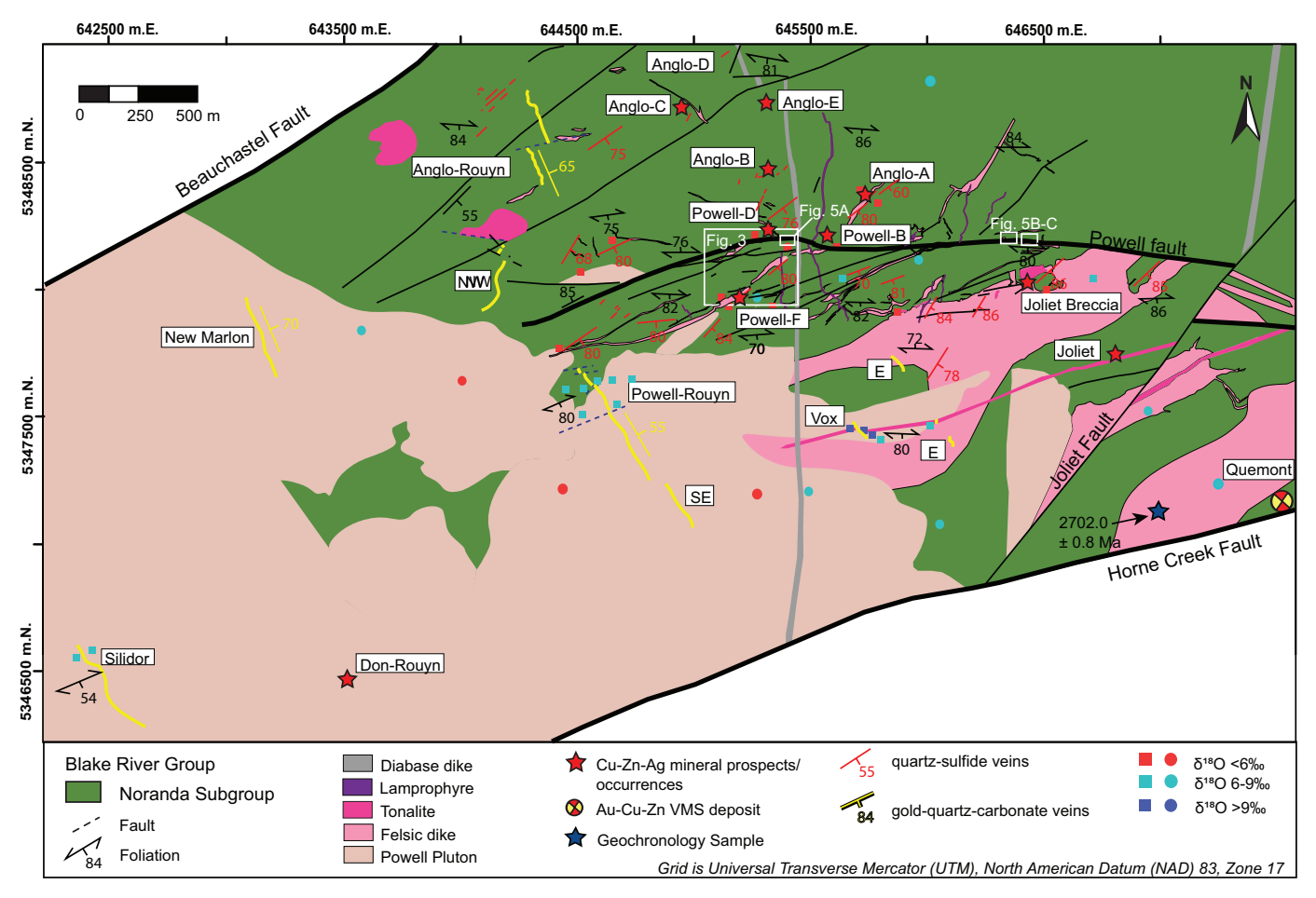


Fig. 2. Geologic map of the Powell block, modified from H.R. Morris (unpub. maps, 1957, 1959), showing the distribution and orientations of the gold quartz-carbonate veins (yellow) and quartz-sulfide Cu-Zn-Ag veins (red). Whole-rock $\delta^{18}O$ data localities from this study and previous studies (Cathles, 1993; Taylor et al., 2014) are shown by squares and circles, respectively, color coded to reflect the typical ranges used for volcanogenic massive sulfide (VMS) exploration in the district (Cathles, 1993; Taylor et al., 2014). Note the higher whole-rock $\delta^{18}O$ values proximal to the gold quartz-carbonate veins and lower whole-rock $\delta^{18}O$ values proximal to the quartz-sulfide Cu-Zn-Ag veins. White boxes show historical and informal deposit and vein names

canic rocks as evidenced by the Joliet breccia and related Cu mineralization (Schofield et al., 2021).

Numerous felsic, mafic, and composite dikes occur throughout the Powell block. They typically strike east-northeast and coincide with stratigraphic offsets. A quartz-feldsparporphyritic rhyolite dike was dated at 2702.0 ± 0.8 Ma (Fig. 2; McNicoll et al., 2014). Younger lamprophyre, mafic, and syenite dikes strike north-northeast to north-northwest and crosscut the Powell intrusion E-NE–striking dikes and all volcanic strata within the Powell block. Proterozoic diabase dikes crosscut all units as well as most faults (Fig. 2) and represent the youngest intrusive event (Carrier et al., 2000).

Rocks of the Powell block have undergone higher strain than the northern Flavrian block of the Noranda volcanic complex (Dimroth et al., 1983; Hubert et al., 1984). In the Powell block, the D_1 event is not expressed by mesoscopic and macroscopic structural features and may simply have contributed to the moderate eastward dips of the volcanic strata. Later deformation events imparted structural fabrics on the rocks of the Powell block and are described below.

Structural Analysis

The D₂ deformation event produced the most prominent structures in the Powell block, including the Powell syncline (Fig. 3), a regional cleavage, a shape and mineral stretching lineation, a bedding-cleavage intersection lineation, and major E-W-striking brittle-ductile shear zones (Fig. 4A-F). The regional S2 cleavage is present across the Powell block but is more prominent in hydrothermally altered rocks, where it is expressed as a penetrative continuous slaty cleavage defined by chlorite and sericite. In weakly to moderately altered massive felsic rocks, it forms an anastomosing sericitic fabric that imparts a pseudoclastic appearance to the rocks. Pillows in volcanic flows, clasts in volcaniclastic units (Fig. 4A), and ovoid metasomatic spots (Fig. 4B) are flattened parallel to the S₂ cleavage and elongate parallel to an L₂ shape stretching lineation. The mineral stretching lineation is restricted to E-W-striking shear zones (Fig. 5A-D) and defined by yellow grooves of sericite and ribs of quartz. Structural measurements of bedding, lineations, and cleavage were taken along the limbs and hinge of the F₂ Powell syncline. Poles to folded

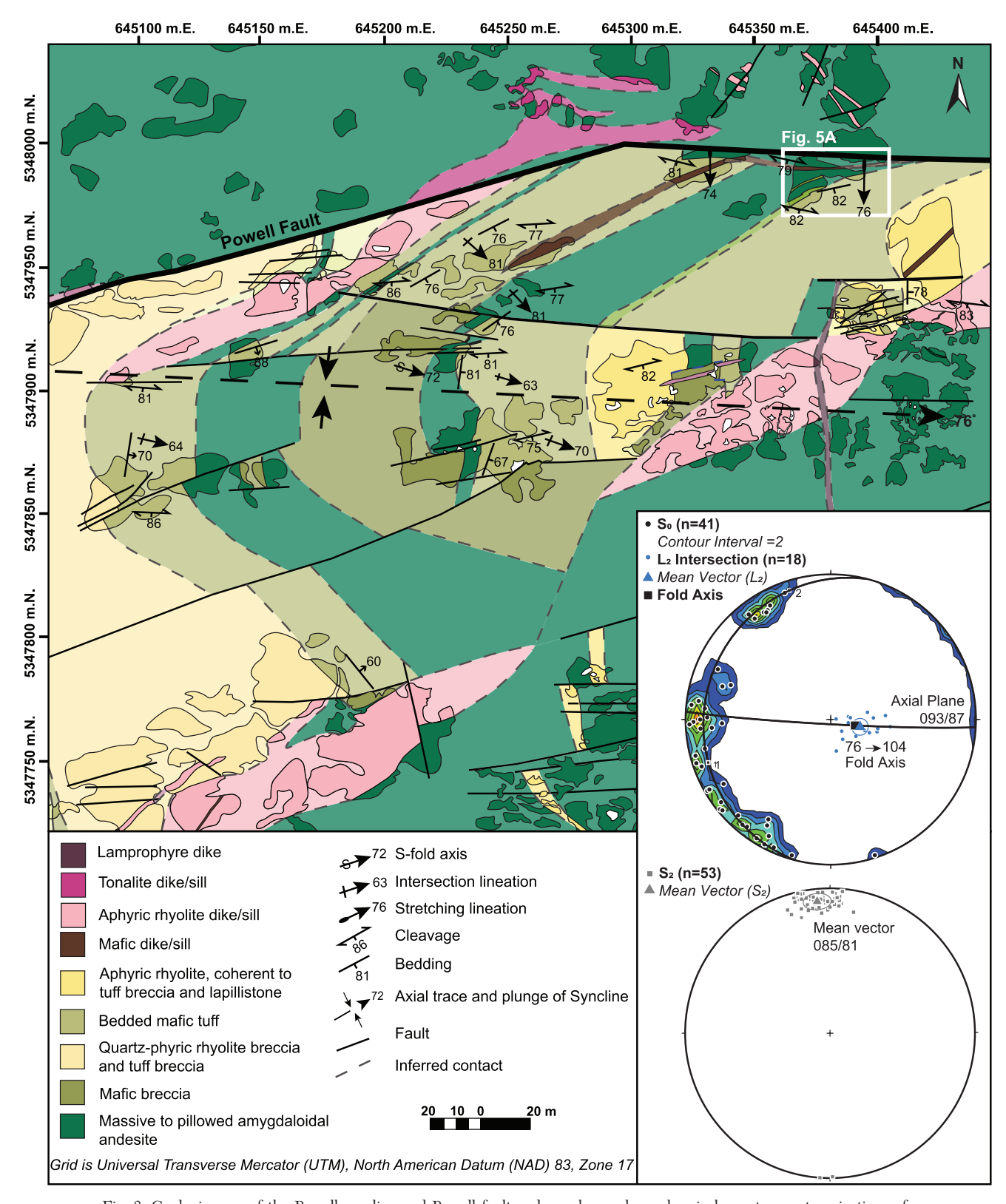


Fig. 3. Geologic map of the Powell syncline and Powell fault and equal area, lower hemisphere stereonet projections of structural measurements from the Powell syncline; stereonet plots generated with Stereonet (Allmendinger et al., 2012). The trend and plunge of the fold axis have been interpreted from the pole to the great circle that best fits the distribution of poles of bedding measurements. Contours of poles to bedding measurements are calculated as a percentage of the total number of data points per 1% of area with contour intervals of two. The calculated fold axis orientation overlaps with the mean vector of the measured intersection lineations between bedding and foliation. The orientation of the axial plane was determined from its mapped surface trace combined with the computed fold axis.

Table 1. Zircon U-Pb Isotope Data for Tonalite Intrusions

Fraction	Description	U (ppm)	$Pb^{T}\left(pg\right)$	$\mathrm{Pb}_{\mathrm{C}}(pg)$	Th/U	²⁰⁶ Pb/ ²⁰⁴ Pb	$^{206}Pb/^{238}U$	± 2σ
20MDS-186	20MDS-186B, tonalite dike crosscuts Joliet Cu deposit and overprinted by ankerite and hematite alteration at Vox occurrence							
Z1	1 clr, cls, blocky frag	259	110.26	0.38	0.617	15,802	0.522503	0.001091
$\mathbb{Z}2$	1 clr, cls, blocky frag	130	80.56	0.84	0.612	5,273	0.530245	0.001096
Z 3	1 elr, els, brkn half-pr	326	194.48	2.75	0.512	3,998	0.523305	0.001459
20MDS-201B, tonalite overprinted by stockwork and disseminated Cu mineralization, D-zone Cu occurrence								
Z1	1 clr, cls, sharp, fetd, brkn pr	196	115.22	0.11	0.468	57,313	0.520385	0.000996
$\mathbb{Z}2$	1 euh, clr, cls, 2:1 pr	65	37.99	0.20	0.405	10,968	0.526845	0.001295
Z 3	1 lrg, clr, cls, brkn, gemmy pr	230	135.08	0.58	0.477	13,171	0.519373	0.001008
Z4	1 sm, clr, cls, gemmy, 2:1 pr	175	51.76	0.33	0.472	8,850	0.522480	0.001188

Notes: All analyzed fractions represent best optical quality (inclusion- and core-free) fresh (least altered) grains of zircon; zircons were chemically abraded; Pb^{T} is total amount (in picograms) of Pb; Pb_{C} is total measured common Pb (in picograms) assuming the isotopic composition of laboratory blank: $206/204 = 18.49 \pm 0.4\%$, $207/204 = 15.59 \pm 0.4\%$, and $208/204 = 39.36 \pm 0.4\%$; Pb/U atomic ratios are corrected for spike, fractionation, blank, and, where necessary, initial common Pb; $^{206}Pb/^{204}Pb$ is corrected for spike and fractionation; Th/U is model value calculated from radiogenic $^{208}Pb/^{206}Pb$ ratio and $^{207}Pb/^{206}Pb$ age, assuming concordance; Disc (%) is percent discordance for the given $^{207}Pb/^{206}Pb$ age; uranium decay constants are from Jaffey et al., 1971

Abbreviations: brkn = broken, clr = clear, cls = colourless, fctd = faceted, frag = fragment, lrg = larger, pr = prism/prismatic, sm = smaller, Z = zircon

bedding define a great circle whose pole coincides with data points for the bedding-cleavage intersection lineation (Fig. 3) and mineral and shape stretching lineation (Fig. 5C). The lineation data points (average plunge of 73° toward 103°) fall within the plane of the regional cleavage (average strike of 085° and dip of 81°) that bisects the interlimb angle (78°) of the fold. This confirms that the Powell syncline, regional cleavage, and the shape and mineral stretching lineation are coeval F_2 , S_2 , and L_2 structural features, respectively, that formed during the D_2 deformation event.

The Powell syncline is truncated to the north by the Powell fault. The latter is expressed as an ~2- to 10-m-wide, strongly foliated zone that strikes east-southeast (099°) and dips steeply (81°) to the south (Fig. 5). It is characterized by the intensification of the S2 cleavage into a sericitic and chloritic phyllonitic foliation (Fig. 4C) and by a pronounced subvertical mineral stretching lineation, which is parallel to the L2 shape and mineral stretching lineation. This suggests that the Powell fault formed during the D2 deformation event. Shear sense indicators—including sigma-shaped clasts (Fig. 4D), S-C fabrics (Fig. 4E), and shear bands—are observed on vertical surfaces perpendicular to foliation and parallel to lineation. They indicate north-side-up movement parallel to the mineral stretching lineation.

The phyllonitic foliation along the Powell fault is overprinted by dextral shear bands, Z-folded quartz veins, and a penetrative S_3 crenulation cleavage (078°/75°; Fig. 4F). The latter is axial planar to Z-shaped drag folds and is further expressed as a spaced (~2–7 mm) fracture cleavage within massive felsic rocks and weakly to moderately altered basalt and as a continuous, chloritic and sericitic, slaty cleavage in altered basalt. These shear sense indicators, together with the progressive clockwise (~17°) rotation of the S_2 cleavage with increasing proximity to the Powell fault, suggest that the Powell fault was reactivated as a dextral transcurrent fault during a D_3 deformation event.

Cu-Zn-Ag Prospects and Occurrences

Copper-zinc-silver prospects and minor occurrences are abundant in the Powell block northwest of the Joliet breccia

(Fig. 2). Although all were studied in detail, only the Powell F-zone and Powell D-zone (Fig. 6) data are presented here because they are representative of the range of host-rock compositions and hydrothermal features observed at all of the Cu-Zn-Ag prospects.

The Powell F-zone occurrence consists of an ~1-m-wide quartz, chalcopyrite, pyrite, sphalerite vein with a strike length of 90 m (Fig. 6). The vein occurs along the margin of a 30-m-wide NE-striking, aphanitic, aphyric, spherulitic, felsic dike (Fig. 6). The dike has irregular lobate flow banded to brecciated margins, and the vein crosscuts both its brecciated margin and more massive interior. The felsic dike marks a distinctive stratigraphic offset. The regional E-W-striking S₂ cleavage overprints both the felsic dike and the vein. The vein strikes northeast (056°) and dips steeply (80°) to the southeast (App. Fig. A1). The vein pinches and swells along strike and is locally offset by E-W- and NNW-striking faults. Smaller (5- to 20-cm-wide), oblique (030°) quartz-sulfide veins that branch off from the main vein are also offset by a brittle E-W-striking fault. The S₂ cleavage overprints the brittle fault and wraps around the competent segments of the offset vein. Disseminated sulfide minerals in the host rocks within 8 m of the vein give the rock a rusty weathered appearance.

The Powell D zone consists of an ~150- by ~90-m area of predominantly fracture-controlled to disseminated sulfide minerals. It is located on the west side of a NE-striking fault infilled by a sulfide vein (Fig. 6). The vein is ~30 cm wide and has a strike length of ~70 m and is enveloped by an ~7-m-wide zone of stockwork to disseminated sulfide minerals. The vein terminates to the southwest in a branching network of sulfide veins and disseminated sulfides. The large area of disseminated to fracture-controlled mineralization is characterized by a concentric distribution of sulfides in plan view decreasing in abundance from the center outward (Fig. 6). Its mineralized center is a breccia consisting of angular vuggy patches of quartz and sulfide minerals between angular fragments of the host andesite. The breccia is surrounded by a zone of disseminated to fracture-controlled mineralization, itself surrounded by a zone of weakly mineralized, dominantly fracture-controlled mineralization. The fractures typically

1	 . /	-	
Tab	- (('01	n+)

					Ages (Ma)						
Fraction	²⁰⁷ Pb/ ²³⁵ U	± 2σ	²⁰⁷ Pb/ ²⁰⁶ Pb	± 2σ	²⁰⁶ Pb/ ²³⁸ U	± 2σ	²⁰⁷ Pb/ ²³⁵ U	± 2σ	²⁰⁷ Pb/ ²⁰⁶ Pb	± 2σ	Disc (%)
Z1	13.31029	0.03254	0.184756	0.000165	2709.8	4.6	2701.9	2.3	2696.0	1.5	-0.6
$\mathbb{Z}2$	13.49552	0.03418	0.184591	0.000196	2742.5	4.6	2715.0	2.4	2694.6	1.7	-2.2
Z3	13.32063	0.04250	0.184616	0.000212	2713.2	6.2	2702.6	3.0	2694.8	1.9	-0.8
Z1	13.27214	0.03068	0.184976	0.000148	2700.8	4.2	2699.2	2.2	2698.0	1.3	-0.1
$\mathbb{Z}2$	13.43226	0.03760	0.184912	0.000157	2728.1	5.5	2710.5	2.6	2697.4	1.4	-1.4
Z 3	13.24045	0.03113	0.184894	0.000155	2696.5	4.3	2696.9	2.2	2697.3	1.4	0.0
Z4	13.32392	0.03513	0.184953	0.000173	2709.7	5.0	2702.9	2.5	2697.8	1.5	-0.5

strike northeast and are overprinted by a conjugate set of thin, planar NNW- and E-W-striking sulfide-filled fractures (<1 mm in thickness) that have no discernible alteration halo.

The host rocks at the Powell D zone consist of massive andesitic flows striking approximately west-northwest and dipping moderately to the north-northeast. Several WNW-striking intrusions cut the andesitic flows, including ≤1-m-thick, subparallel, aphyric, spherulitic, flow-banded rhyolite sills/dikes, and a larger, irregular quartz- (1–2 mm; 20%) feld-spar- (2–3 mm; 30–40%) porphyritic tonalite intrusion that is overprinted by the sulfide mineralization. The tonalite intrusion contains fine-grained disseminated sulfides, and its outer margin is locally marked by a pronounced ~0.5-m-wide zone of sheeted ~1-mm-wide sulfide fractures that are oriented perpendicular and parallel to the tonalite contact and locally crosscut the tonalite.

There is no compliant estimate of tonnage and grade for these prospects and occurrences. A. Lichtblau (unpub. report, 1979) provided a noncompliant estimate of 22,680 tonnes (t) of mineralization at a grade of 7.88% Cu, 118.3 g/t Ag, and 0.24 g/t Au for the Powell F-zone occurrence. Grab samples from this study of the Powell F-zone and Powell D-zone veins assayed 1.6% Cu, 0.5 ppm Au, 43.6 ppm Ag, and 0.11% Zn; and 1.3% Cu, 0.14% Zn, and 16.4 ppm Ag, respectively (Table A1). Three grab samples of the disseminated mineralization at Powell D zone averaged 0.08% Cu, 0.2 ppm Au, 6 ppm Ag, and 0.04% Zn (Table A1). The metal tenor for these prospects and occurrences is similar to that of the Joliet breccia (Schofield et al., 2021) and overlaps with the typical range for Cu-Zn VMS deposits (e.g., Franklin et al., 1981; Fig. 7).

Cu-Zn-Ag vein petrography and paragenesis

The Cu-Zn-Ag veins are zoned and consist of an outer banded margin and an inner vuggy and porous center. The outer vein margin is locally banded by alternating thin slivers of altered wall rock and bands of quartz with lesser pyrite and chalcopyrite (Fig. 8A, B). The banding is commonly asymmetrically developed, e.g., at Powell F zone, and in some places only occurs at the margin between the vein and the more competent felsic dike. Where banding is not present, there is a gradation between the medium-grained, vuggy, white quartz margin of the veins and the sulfide-dominated center of the veins (Fig. 8C). The vein centers consist of massive pyrite ± pyrrhotite ± chalcopyrite and minor fine-grained gray quartz surrounding rare fragments of altered wall rocks and inclusions of white quartz (Fig. 8B, C). Similar textures are observed in the brec-

cia at the Powell D zone, but the mineral infill is restricted to angular vugs between clasts of altered wall rock (Fig. 8D). The observation of quartz-dominant vein margins grading inward to a pyrite-dominant core suggests that pyrite was deposited later than the quartz. The banded margins and presence of fragments of quartz and altered wall rock internal to the veins suggest that there may have been multiple periods of dilation—opening of the veins and fractures—and subsequent mineral deposition and sealing. Pyrite, in the center of the vein, consists of angular fragments with jigsaw-fit margins (Fig. 8B) and more rounded fragments with corroded and abraded grain surfaces. Microfractures transect the grains in both cases (App. Fig. A2A-D). Anhedral inclusions of galena, sphalerite, chalcopyrite, and Ag and Bi tellurides occur as small blebs that align with the fractures and in vugs (App. Fig. A2A-F). The mineral associations, textures, and paragenesis for the Cu-Zn-Ag prospects are similar to those for the Joliet breccia (e.g., Schofield et al., 2021) and are typical of Cu-Zn VMS deposits (e.g., Franklin et al., 1981).

Hydrothermal alteration associated with Cu-Zn-Ag veins

Two main types of alteration (Fig. 8E-H) surround all the Cu-Zn-Ag occurrences: fine-grained chlorite and spotted sericite-chlorite (Fig. 6). Both overprint an older, more pervasive, and district-scale spilitic (albite-chlorite) alteration (Gibson et al., 1983; Hannington et al., 2003; Fig. 6).

Albite-chlorite alteration (spilitization): All volcanic units within the study area have undergone an early spilite alteration. This alteration is characterized by quartz, albite, chlorite, and rutile and is locally observed as relic patches within chlorite and spotted sericite-chlorite alteration zones (e.g., Schofield et al., 2021). Epidote is rare, and actinolite is only present locally as a pseudomorph of pyroxene phenocrysts within medium- to coarse-grained massive porphyritic mafic flows or intrusions. Chlorite is typically Mg rich (Mg-pycnochlorite), exhibits anomalous brown-blue birefringence, and is interstitial to albite microlites. This spilitic alteration is pervasive throughout the Rouyn-Noranda district and has been interpreted to be a product of the interaction between volcanic rocks and relatively cold down-drawn seawater within a shallow, subseafloor hydrothermal system (Gibson et al., 1983; L'Heureux, 1992; Franklin et al., 2005; Schofield et al., 2021).

During this alteration, albite, pycnochlorite (Fig. 9), and quartz formed at the expense of primary volcanic glass, calcic feldspar, epidote, and clinopyroxene. Lithogeochemical data show these rocks have distinctive high- Na_2O and low-

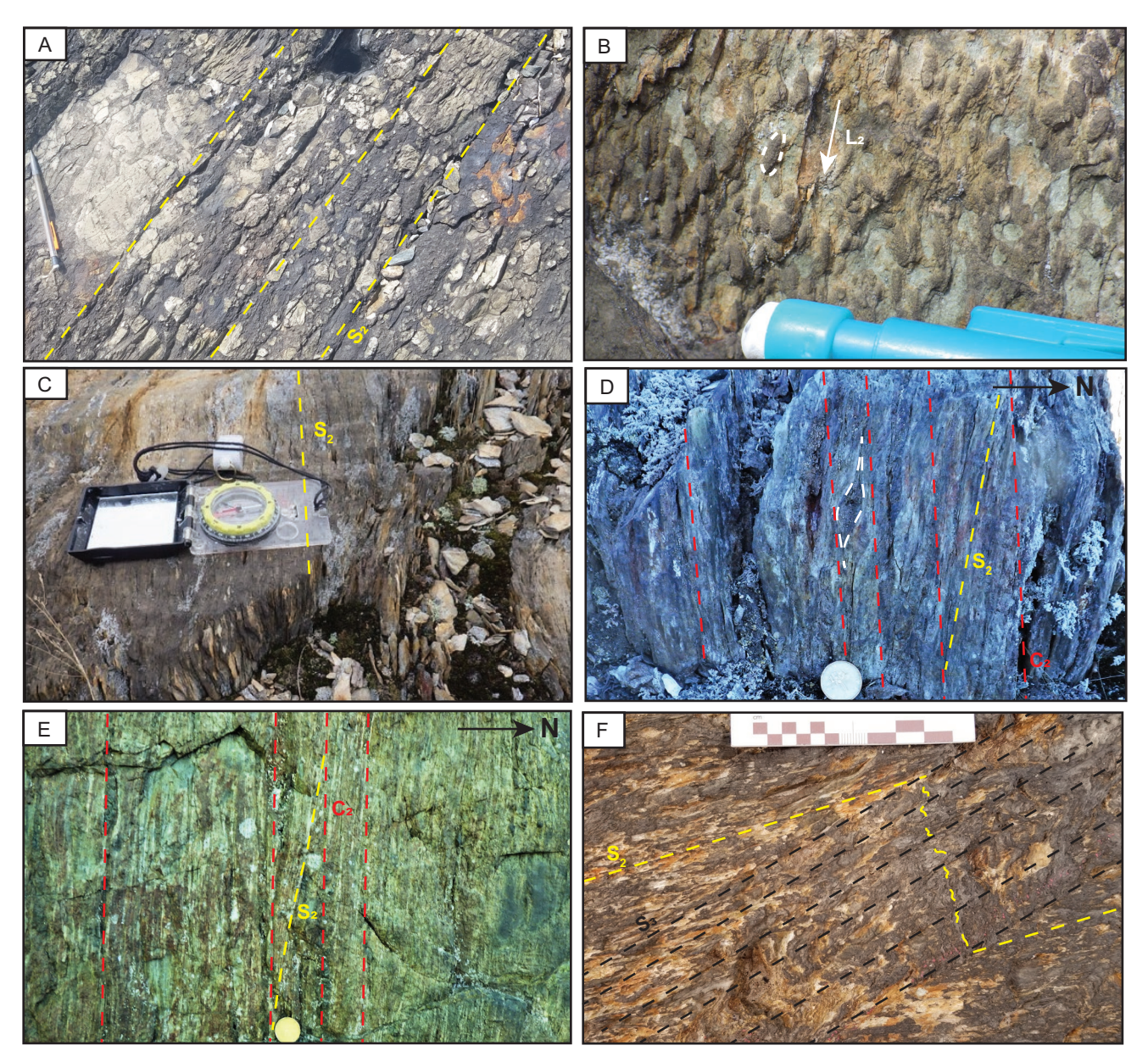


Fig. 4. Outcrop photographs of the main structural elements of the D_2 and D_3 deformation increments within the Powell block. (A) The S_2 foliation defined by elongate and aligned clasts in weakly altered rhyolite lapillistone. (B) Deformed spotted alteration in the Powell fault showing a subvertical shape lineation of individual spots. (C) Sericitic phyllonitic S_2 fabric within the Powell fault. (D) Vertical surface across the Powell fault showing S-C fabrics and asymmetrical sigmoidal clast indicating north over south movement. (E) Vertical view of the Powell fault showing S-C fabrics indicating north over south movement. (F) S_2 foliation crenulated by S_3 spaced cleavage within the Powell fault.

 K_2O compositions that are typical of spilites (App. Fig. A3; Hughes, 1973).

Spotted (sericite-chlorite) alteration: The background regional spilite alteration is locally overprinted by discordant spotted sericite-chlorite alteration. This is a fracture-controlled alteration, which is commonly observed as 4- to ~30-cm-wide halos surrounding sulfide veinlets (Fig. 8E, F). This alteration occurs in association with the Cu-Zn-Ag veins and as a 0.5-m-wide halo surrounding the younger tonalite intrusion at the Powell D zone. The spots visually resemble varioles and consist of ovoid clusters (0.2–1 cm diam) of fine-grained sericite (muscovite) within a chlorite-altered matrix (Fig. 8G,

H) and can be distinguished from varioles by their localization along discordant fractures and veins. Contacts between the ovoid sericite clusters and the chloritic groundmass are typically diffuse (Fig. 8G). The sericite clusters are observed distal to veins as very small spots (2–3 mm diam) that merge into larger spots (0.5–1 cm diam) with increasing proximity to the veins (Fig. 8G) and are associated with a concomitant increase in chlorite in the groundmass at the expense of albite microlites. These clusters are typically concentrically zoned with albite- and muscovite-rich cores, surrounded by muscovite- and chlorite-rich margins (Fig. 8G, H). The original composition of the host rock controls the composition of the

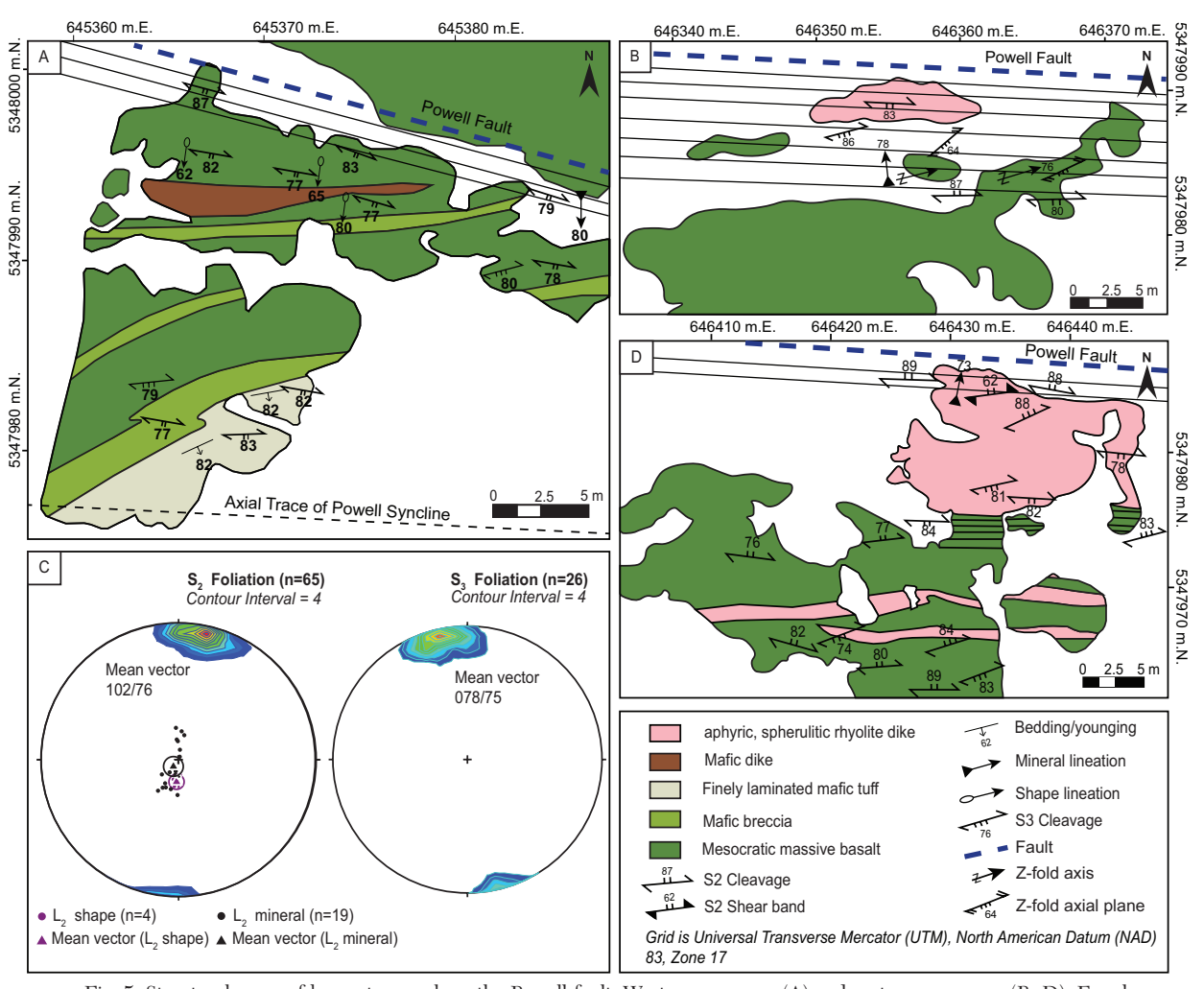


Fig. 5. Structural maps of key outcrops along the Powell fault. Western exposure (A) and eastern exposures (B, D). Equal area, lower hemisphere, stereonet projections (C) summarize foliation and lineation measurements along the Powell fault. Stereonet plots generated with Stereonet (Allmendinger et al., 2012). Contours of poles to bedding measurements are calculated as a percentage of the total number of data points per 1% area with contour intervals of four.

chlorite, with chlorite found in spotted felsic rocks exhibiting a higher Fe content than chlorite in spotted mafic rocks (Fig. 9). The only phase preserved in the matrix from the precursor spilitized host rock is fine-grained disseminated quartz, which also occurs as inclusions within the spots. This alteration results in gains in K \pm Fe and losses in Na \pm Mg (App. Fig. A3).

Ankerite locally overprints spotted andesite in crosscutting quartz-carbonate veinlets and as disseminated carbonate. Fine-grained, euhedral to subhedral ankerite typically occurs along the outer margins of alteration spots where it replaces fine-grained muscovite.

Chlorite alteration: Massive, discordant, and fracture-controlled chlorite alteration is best developed immediately adjacent to the Cu-Zn-Ag veins (Fig. 8F). The chlorite is fine grained and replaced the groundmass in coherent mafic and felsic volcanic flows and hypabyssal intrusive rocks. It is more laterally extensive in permeable volcaniclastic units where it has replaced the hyaloclastite and tuffaceous matrix between more competent clasts. It overprints and is in sharp contact with the spotted alteration texture (Fig. 8F). This pervasive

chlorite alteration is texturally destructive and has obliterated preexisting feldspar microlites or phenocrysts. The only other mineral phases that occur with the fine-grained chlorite (60%) are disseminated, fine-grained, subhedral quartz (25%) and subhedral to euhedral rutile (15%). Chlorite is Fe rich and the replacement of muscovite by Fe-rich chlorite reflects gains in Fe, Mg, and $\rm H_2O$ and losses in K (App. Fig. A3).

Au Deposits and Occurrences

Gold deposits in the Powell block are dominantly confined to the Powell intrusive complex and are typically associated with NNW-striking mafic dikes. Several of the historically mined veins are no longer accessible; however, the two best surface exposures, Silidor and Vox (Fig. 10A-E), were studied in detail to characterize this style of mineralization.

The Silidor vein strikes on average 330° and dips 50° east-northeast (App. Fig. A1) with an average width of ~3.5 m. It is located within tonalite of the Powell intrusive complex (Fig. 2) in association with highly altered mafic dikes (Fig. 10A). Tonalite in immediate proximity to the vein is heavily

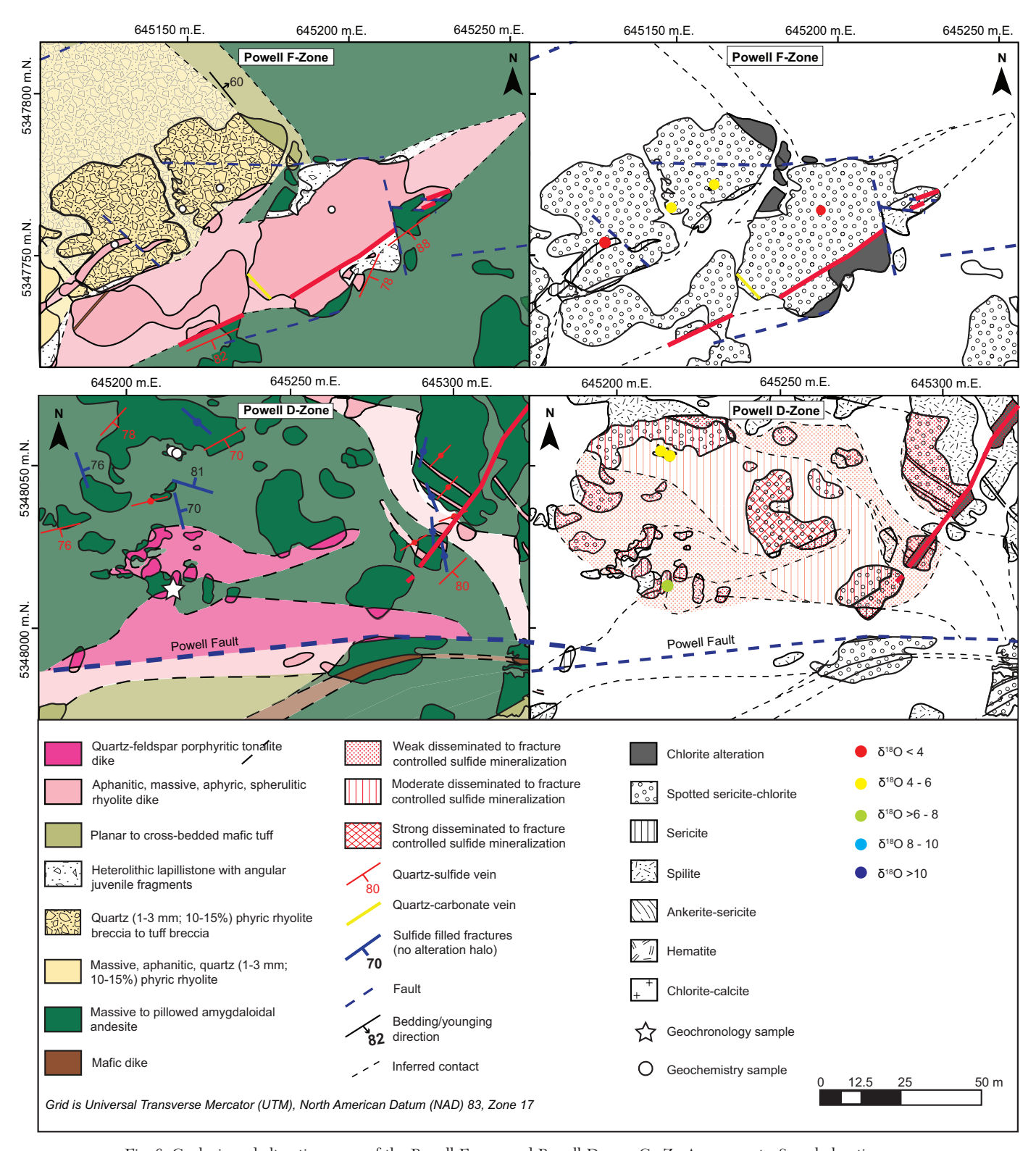


Fig. 6. Geologic and alteration maps of the Powell F-zone and Powell D-zone Cu-Zn-Ag prospects. Sample locations are shown in white circles for whole-rock geochemistry and $\delta^{18}O$ analysis. Whole-rock $\delta^{18}O$ values are color coded to reflect their variation. Note the alteration associated with these veins extends into the host rocks for ~100 m from the veins and is associated with whole-rock $\delta^{18}O$ values <7‰. The white star shows the location for tonalite dike U-Pb geochronology sample 20MDS-201B in the Powell D zone.

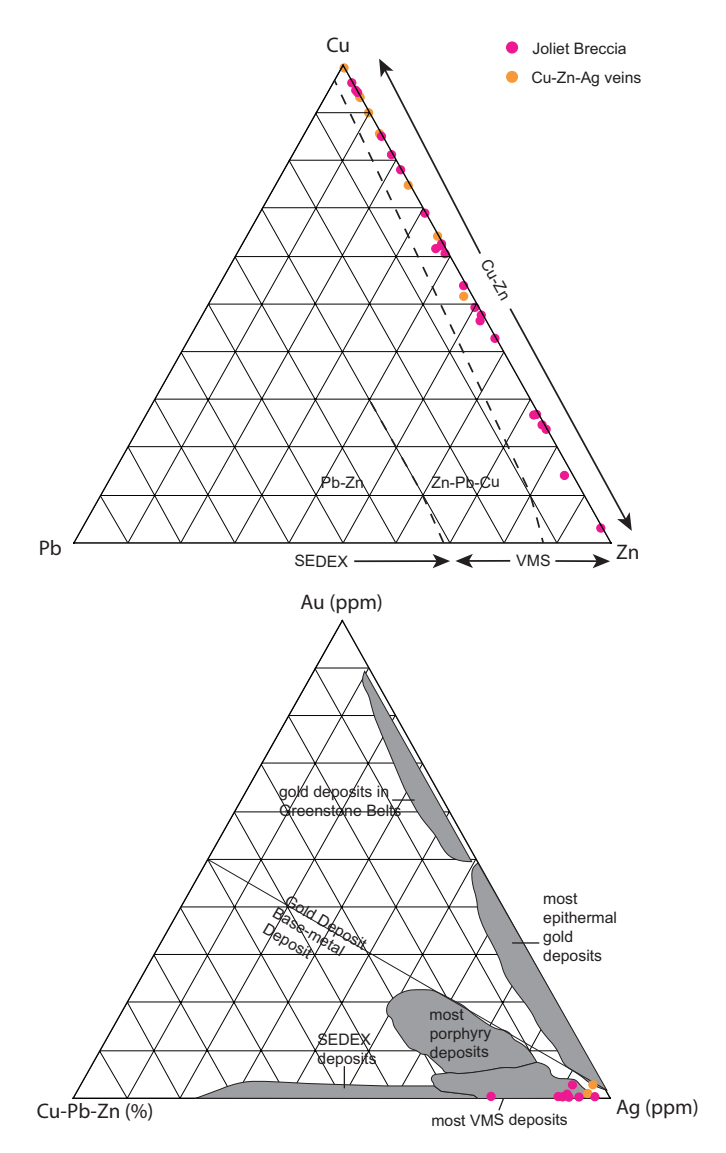


Fig. 7. Ternary plots modified from Franklin et al. (1981) and Hannington et al. (1999) showing the metal tenor of the Cu-Zn-Ag veins compared to the Joliet breccia (Schofield et al., 2021) and typical base metal deposits. The veins and Joliet breccia overlap with the Cu-Zn VMS field. Abbreviations: SEDEX = sedimentary exhalative, VMS = volcanogenic massive sulfide.

fractured and contains numerous ~1-mm-wide anastomosing fractures filled with chlorite and carbonate and trace amounts of disseminated pyrite.

The contact with the vein is marked by a carbonate-fuch-site breccia, comprising altered, locally jigsaw-fit fragments of tonalite in a carbonate, chlorite ± quartz matrix with trace amounts of disseminated pyrite and fuchsite (Fig. 11A). Several parallel, thin, secondary quartz veins are hosted by the breccia and mafic dike(s) (Fig. 11B). In addition, numerous 1- to 2-cm-wide, NNE-striking (Fig. A1), fibrous quartz ± ankerite ± specular hematite veins crosscut the host rocks (Fig. 11C, D) and the main north-northwest quartz vein, but are also locally folded and rotated into the footwall of the vein. The main Silidor vein and parallel secondary veins are folded (Fig. 11B, C) into open, moderately NE-plunging folds with an interlimb angle of ~120°. The regional E-W-striking and

steeply S-dipping cleavage is oriented at a high angle $(45^{\circ}-90^{\circ})$ to the folded vein and is axial planar to the folds (Fig. A1). This cleavage is most strongly developed in the mafic dike and carbonate matrix of the footwall breccia where it is expressed as a spaced and anastomosing cleavage defined by chlorite (Fig. 11A, D). Late E-W-striking sinistral and dextral faults offset the Silidor vein laterally by up to 50 m (Carrier et al. 2000).

The Vox vein is hosted by an older quartz- (~5%; 0.5–1 mm) feldspar- (1%; 0.5-1 mm) porphyritic rhyolite dike, which is cut by the Powell quartz-diorite and a porphyritic tonalite dike (Fig. 10B). The vein does not coincide with a mafic dike but with a structure that dextrally offsets by 20 m in map view the porphyritic tonalite dike. The Vox vein is on average 1 to 2 m thick, but it pinches and swells (up to 5 m thick) along strike. Where thickest, it contains angular altered wall-rock fragments. There are several smaller, 10- to 20-cm-wide, subparallel quartz-breccia veins that crosscut the host rocks in the hanging wall up to ~100 m away from the main Vox vein. These veins are all folded into open, moderately E-plunging folds and crosscut by an E-W-striking, steeply dipping cleavage. Extensional, NNE-striking, subvertical, fibrous quartz ± ankerite ± specular hematite veins, varying in width from 7 to 12 cm, cut across the NNW-striking veins and are locally folded and rotated into the veins and parallel structures.

Gold quartz-carbonate vein petrography and paragenesis

The gold quartz-carbonate veins have a white quartz banded (Fig. 11E) to brecciated (Fig. 11F) outer margin and a massive, white to smoky gray, quartz inner center. Locally, sulfide minerals fill vugs lined with quartz (Fig. 11G). Pyrite grains in the veins and the altered wall rocks are subhedral to euhedral and are internally porous. Aggregates of pyrite grains locally exhibit annealed textures with triple-point terminations (App. Fig. A4). Gold occurs in the veins and altered wall rocks as electrum inclusions and pore fillings in pyrite, along fractures transecting pyrite grains, and along pyrite grain boundaries (App. Fig. A4) in association with chalcopyrite, galena, and tellurides as anhedral intergrown blebs (App. Fig. A4). Pyrite also contains inclusions of apatite, quartz, rutile, muscovite, chlorite, and ferroan dolomite (App. Fig. A4) that formed during the alteration of the vein wall rocks as described below.

Hydrothermal alteration associated with gold quartz-carbonate veins

Alteration associated with the gold quartz-carbonate veins consists of chlorite, hematite, albite, carbonate (ankerite and calcite), fuchsite, and sericite. The abundance of these minerals changes with proximity to the veins and to some degree by the composition of the immediate host rocks (Fig. 10C, D). Apatite, rutile, and pyrite are accessory phases observed in all alteration types.

Chlorite-calcite-albite alteration: This is the most distal alteration. It extends from ~30 to 300 m from the vein margins (Fig. 10C). It consists of fine-grained groundmass chlorite, calcite, and albite and gives the rock a dark-green appearance. Chlorite is Mg rich (Mg pychnochlorite/ripidolite) relative to chlorites associated with the Cu-Zn-Ag veins (Fe-pychnochlorite/ripidolite) and tends to be more enriched in Mg in mafic rock units and in Fe in felsic rock units (Fig. 9). It is also rela-

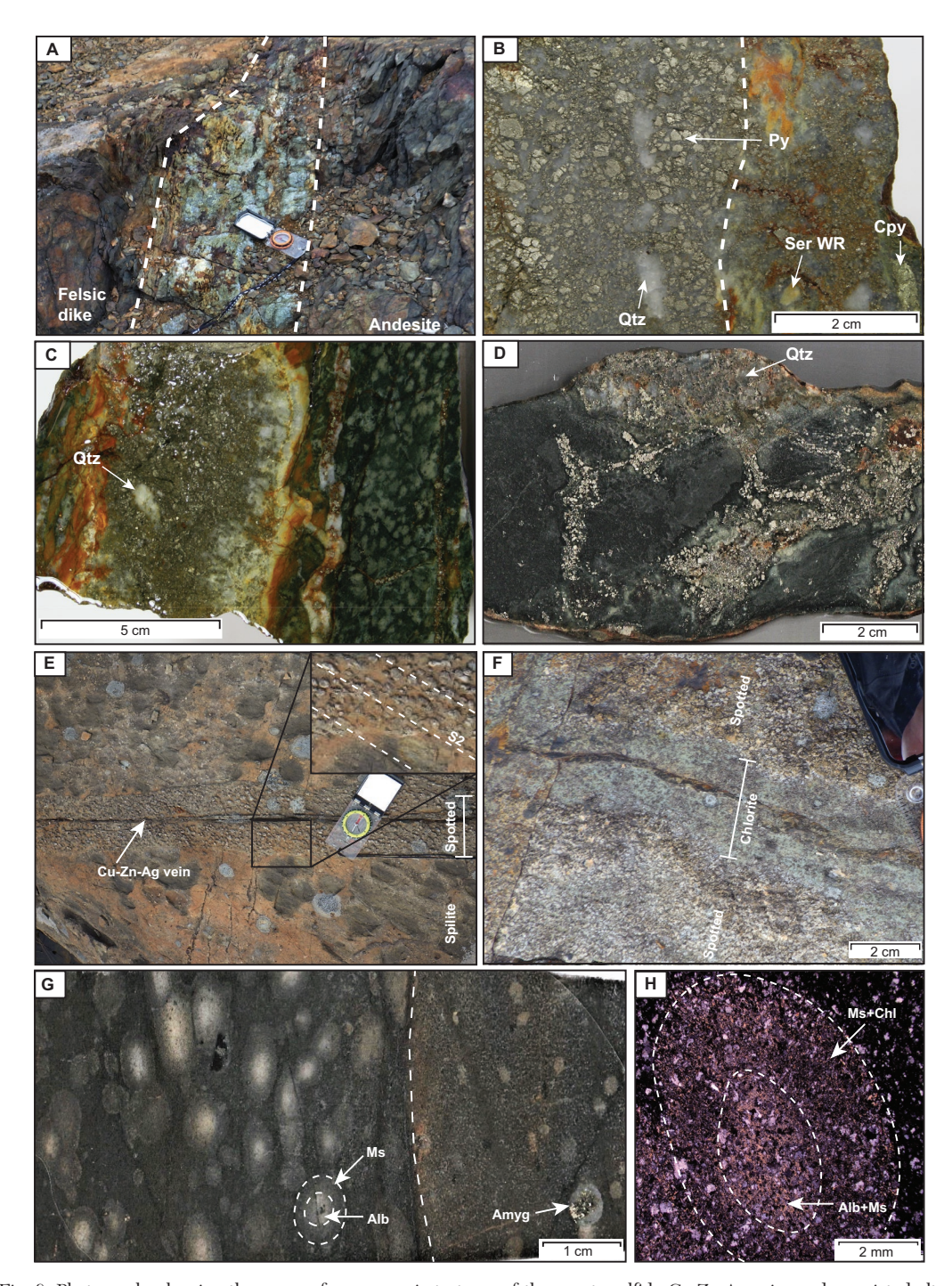


Fig. 8. Photographs showing the range of macroscopic textures of the quartz-sulfide Cu-Zn-Ag veins and associated alteration. (A) Powell F-zone vein, showing outer banded margin adjacent to aphyric rhyolite dike and more massive interior. (B) Anglo D-zone vein with angular jigsaw-fit pyrite and fine-grained gray quartz. Note the angular fragments of white quartz and sericitized wall rock. (C) Anglo D-zone vein showing white, medium-grained, euhedral quartz along the sharp planar margin of the vein with host andesite, and a massive pyrite-dominant core with an angular fragment of quartz. Note the spotted alteration texture in the host andesite. (D) Powell D zone showing angular fragments of andesite cemented by quartz and pyrite. (E) Quartz-sulfide Cu-Zn-Ag vein with associated halo of spotted sericite-chlorite alteration crosscutting spilitized andesite of the Powell F-zone area. Note the very sharp contact of the alteration halo and overprinting S_2 cleavage, which corresponds to shortening of the alteration spots in a direction perpendicular to it (the larger beige and gray patches represent lichen on the outcrop surface). (F) Quartz-sulfide Cu-Zn-Ag vein from the Anglo A zone. Note the alteration zoning from a marginal halo of spotted sericite-chlorite alteration to a proximal Fe-rich chlorite alteration and the overprinting S_2 cleavage. (G) Channel sample through contact between spotted alteration halo and spilitized amygdaloidal andesite from the Powell F zone. Note the concentric zoning of the alteration spots with white albite- and muscovite-rich cores and beige muscovite- and chlorite-rich rims in a chloritized groundmass (polished slab). (H) Close-up of concentrically zoned alteration spot. Abbreviations: Alb = albite, Amyg = amygdule, Chl = chlorite, Cpy = chalcopyrite, Ms = muscovite, Py = pyrite, Qtz = quartz, Ser WR = sericitized wall rock.

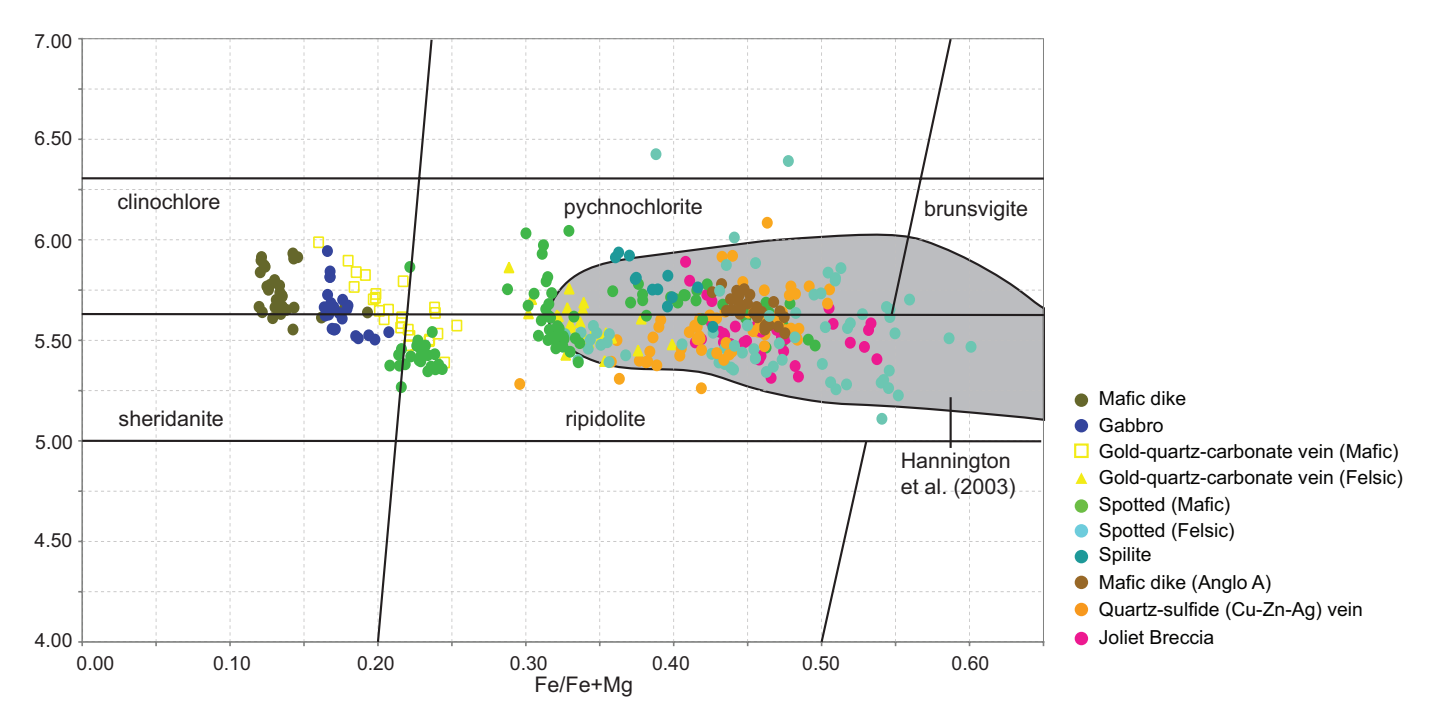


Fig. 9. Scanning electron microscope-energy dispersive spectrometry mineral chemistry results. Chlorite composition and nomenclature for ranges of chlorites from Hey (1954). Felsic protoliths trend toward higher Fe chlorite compositions compared to mafic protoliths, but the highest Fe chlorites occur in both mafic and felsic rock types that are most proximal to Cu-Zn-Ag prospects and occurrences. Chlorite associated with the alteration halos surrounding the Au-deposits are more Mg rich than the chlorite associated with the Cu-Zn-Ag prospects and occurrences. The gray shaded area shows the range of chlorite composition for volcanogenic massive sulfide deposits in Noranda (from Hannington et al., 2003).

tively Fe-rich compared to the chlorite (clinochlore) found in background mafic rocks (mafic dike, lamprophyre, glomero-porphyritic gabbro) (Fig. 9).

Hematite alteration: The chlorite-calcite-albite alteration is overprinted by hematite alteration, which extends for ~ 30 to 200 m into the host rocks (Fig. 10C, D). It is most prominent within tonalite, where it imparts a red-rusty appearance. It consists of fine-grained, disseminated specular hematite ($\sim 25\%$), albite, ankerite, calcite, chlorite, apatite, and rutile \pm ilmenite. It is also concentrated in alteration halos associated with numerous 0.1- to 1-cm-wide brittle fractures in the tonalite and along fracture planes as veinlets of medium-grained specular hematite. This alteration is most abundant in the hanging wall of the veins.

Albite-sericite \pm calcite alteration: This is the most proximal alteration associated with the gold quartz-carbonate veins within highly siliceous felsic host rocks that lack ferromagnesian minerals (e.g., rhyolite flows; App. Fig. A5). It consists of fine-grained granoblastic albite, quartz, muscovite, and calcite within ~30 to 50 m of the veins, imparting a bleached, beige appearance in contrast to the dark-green chlorite-calcite-albite alteration.

Ankerite-sericite \pm fuchsite alteration: This is the most proximal alteration associated with the gold quartz-carbonate veins within the tonalite and mafic dike host rocks (Fig. 10C, D). It consists of ankerite \pm calcite, muscovite \pm fuchsite, albite, and quartz within ~30 to 50 m of the veins, resulting in the rock having a bleached beige coloration (Fig. 11H, I). It is also found in association with E-W-striking brittle-ductile

shear zones across the Powell block and locally overprints the spotted alteration associated with Cu-Zn-Ag occurrences. Within tonalite, this alteration type consists of $\sim\!25\%$ ankerite, $\sim\!40\%$ quartz, $\sim\!25\%$ albite, $\sim\!5\%$ chlorite, and $\sim\!5\%$ muscovite. It is a texturally destructive alteration, which replaces the primary graphic (feldspar-quartz) texture of the tonalite with fine-grained granoblastic quartz and ankerite (Fig. 111). Similarly, ankerite pervasively replaced the mafic dikes, and at Silidor it forms the matrix of the breccia at the contact between the mafic dike and the quartz vein.

U-Pb TIMS Geochronology

Two felsic intrusive units were sampled for high resolution U-Pb zircon geochronology. The first is a quartz-feldsparporphyritic tonalite dike (sample 20MDS-201B; Fig. 12A-C), which is overprinted by disseminated to stockwork Cu mineralization at the Powell D-zone Cu occurrence. Dating of this unit provides a maximum age limit for the mineralization as well as a temporal context for its emplacement relative to regional VMS-related and younger magmatic-hydrothermal breccia associated magmatism (Schofield et al., 2021). The second dated unit is a tonalite dike that is crosscut by the Vox vein and its associated ankerite-sericite alteration (20MDS-186B; Fig. 12D, E). To the northeast of the Vox occurrence this same dike also crosscuts the Joliet Cu deposit (Fig. 2), which is a steeply plunging deposit of similar morphology, metal tenor, and alteration as that of the Joliet breccia (Schofield et al., 2021). It thus provides a minimum age for Cu mineralization and a maximum age for Au mineralization.

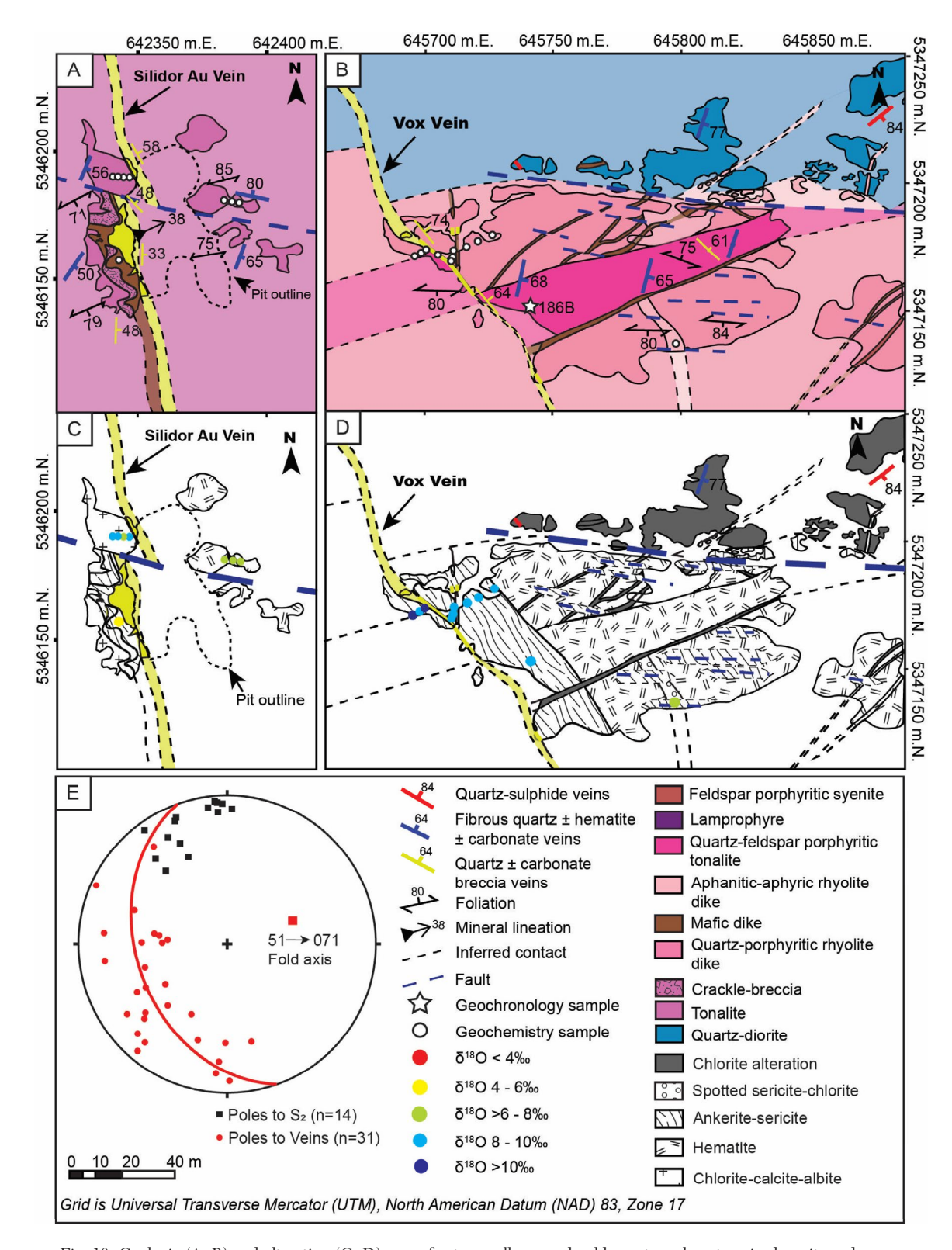


Fig. 10. Geologic (A, B) and alteration (C, D) maps for two well-exposed gold quartz-carbonate-vein deposits and occurrences in the Powell block, Rouyn-Noranda, Quebec. Sample locations are shown in white circles for whole-rock geochemistry and $\delta^{18}O$ analysis. The white star shows the location for the tonalite dike U-Pb geochronology sample, 20MDS-186B, at the Vox occurrence. Whole-rock $\delta^{18}O$ values are color coded to reflect their variations. Note the patches of chlorite and spotted-sericite alteration, overprinted by ankerite-sericite alteration at the Vox occurrence, have relatively high whole-rock $\delta^{18}O$ values compared with the same alteration shown in Figure 6. An equal area, lower hemisphere stereonet projection (E) summarizes structural measurements taken along the gold quartz-carbonate veins (stereonet plots generated with Stereonet; Allmendinger et al., 2012).

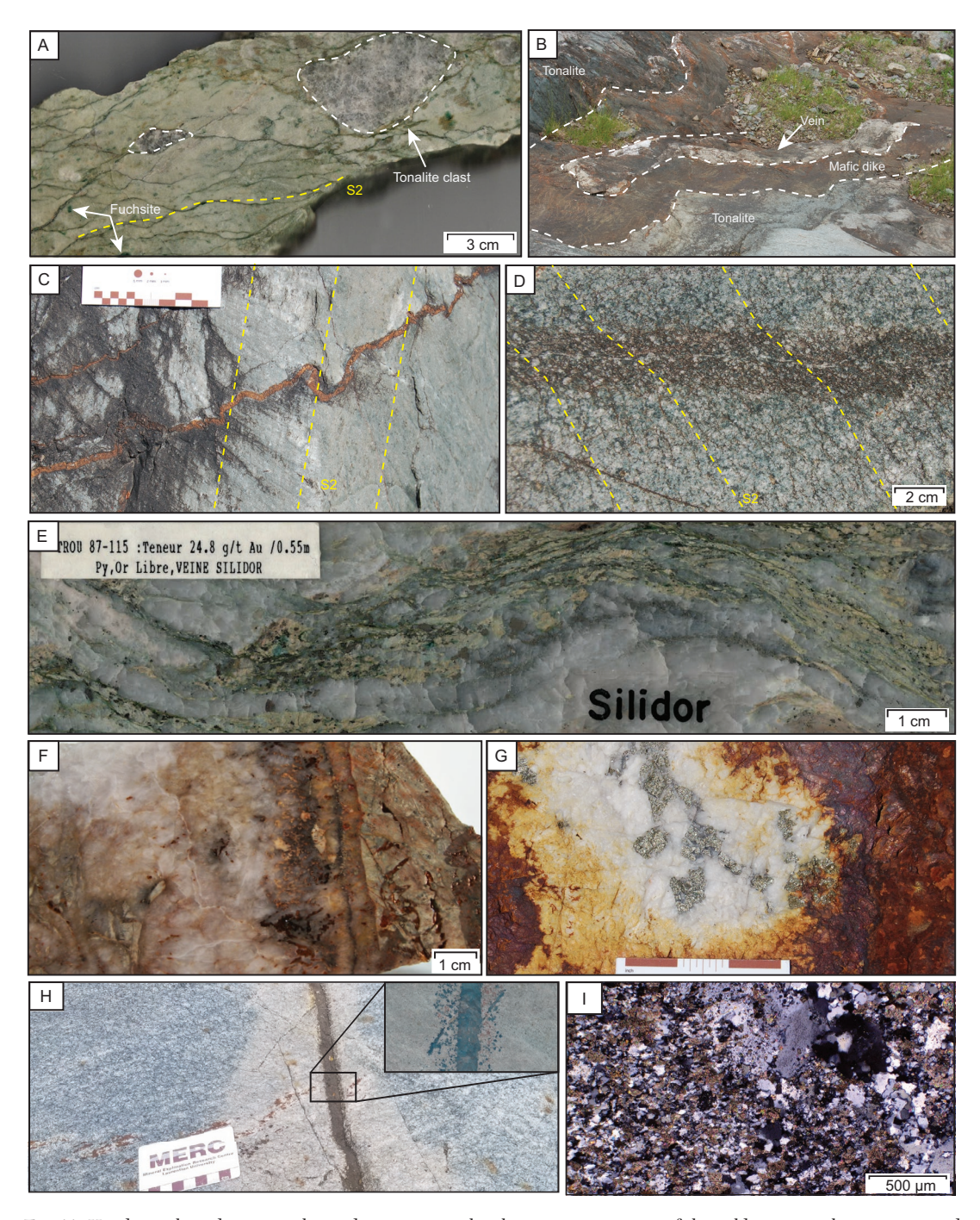


Fig. 11. Hand sample and outcrop photos demonstrating the characteristic textures of the gold quartz-carbonate veins and associated alteration found in the Powell block. (A) Channel sample of carbonate-fuchsite breccia in the footwall of the Silidor vein, with the S_2 cleavage overprinting the matrix of the breccia. (B) Outcrop image of footwall mafic dike and parallel quartz vein, crosscutting tonalite. The thin quartz vein is parallel to the main Silidor vein, and both the dike and the vein are folded into an open, moderately NE-plunging fold. Photo is taken looking down plunge of the fold. Field of view is approximately 2 m. (C) Folded oblique fibrous ankerite veins at the Silidor deposit. (D) Thin quartz veinlet with ankerite-sericite alteration halo crosscutting the hanging-wall tonalite at the Silidor deposit. Note the overprinting cleavage. (E) Historic drill core display sample from hole 87-115. Banded margin of Silidor vein, showing slivers of altered wall rock and disseminated pyrite. Note the folded nature of the vein and the foliated wall-rock slivers. (F) Polished slab of Powell-Rouyn Au vein showing angular altered clasts of host rock within the massive quartz vein. Note the euhedral pyrite within the altered wall rock and the ankerite intergrown with quartz on the margin of the vein (right). (G) Outcrop surface of the vein showing a vuggy texture of quartz with sulfides found internal to the quartz vugs. (H) Chlorite-calcite—altered Powell tonalite from the hanging wall of the Silidor vein, crosscut by a bleached ankerite, calcite, and sericite halo associated with a 1-cm-wide ankerite and hematite vein (outcrop). Inset shows stained (Hitzman, 1999) hand sample with ankerite (blue) and calcite (pink) disseminations surrounding the ankerite vein. (I) Most proximal, intense carbonate alteration in hanging wall of Silidor vein. Graphic textured tonalite completely overprinted by granoblastic carbonate texture.

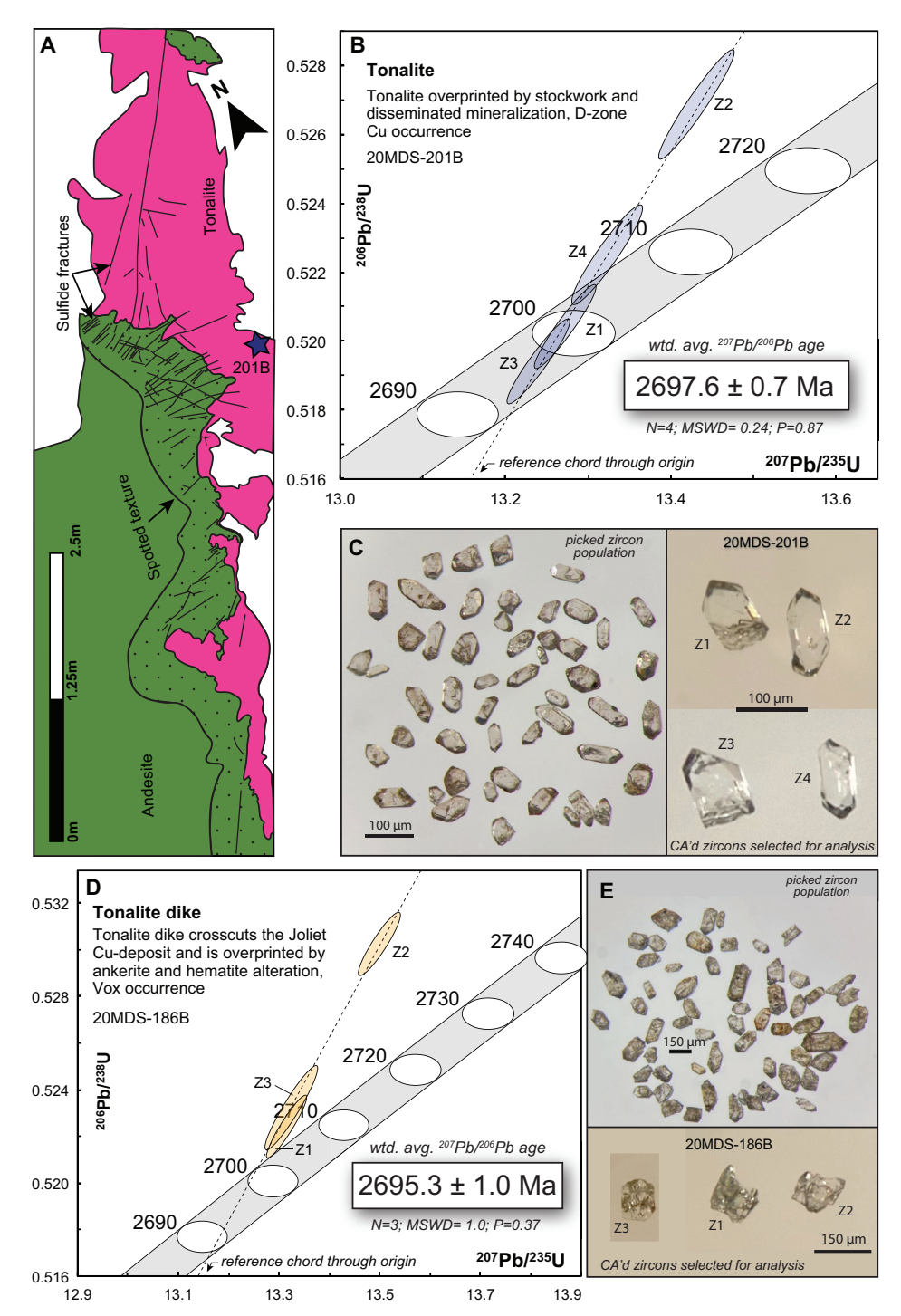


Fig. 12. Results of chemical abrasion (CA)-isotope dilution-thermal ionization mass spectrometry (CA-ID-TIMS) U-Pb analysis of two tonalite samples. (A) Detailed outcrop sketch of tonalite intrusion at Powell D zone from location shown in Figure 3, illustrating the relationship between the sulfide mineralization and the intrusion as well as the location of the geochronology sample. (B) Concordia diagram and (C) zircon grain images for CA-ID-TIMS U-Pb analysis. (D) Concordia diagram for sample of tonalite dike from the Vox gold occurrence (see Fig. 10B for location). (E) Zircon grain images for CA-ID-TIMS U-Pb analysis. Abbreviation: CA'd = chemically abraded.

Zircon recovered from the quartz-feldspar-porphyritic tonalite dike at the Powell D zone yielded a population of small, clear, short, stubby, prismatic, colorless to pale yellow zircon grains (Fig. 12C). A few grains show good oscillatory zoning and small mineral inclusions of apatite and an opaque oxide (ilmenite?). U-Pb isotope analysis of four, best-quality, single grain zircon fractions from sample 20MDS-201B show a linear array of concordant to slightly reverse discordant data, with a narrow range of ²⁰⁷Pb/²⁰⁶Pb ages between 2697.4 and 2698.0 Ma (Table 1, Fig. 12B). Th/U ratios are very consis-

tent (0.41–0.48) and typical of igneous zircons (Kirkland et al., 2015). The data yielded a calculated weighted average $^{207}\text{Pb}/^{206}\text{Pb}$ age of 2697.6 \pm 0.7 Ma (n = 4; mean square of weighted deviates [MSWD] = 0.24; probability of fit = 87%) from the four fractions, which is interpreted to be the crystallization age of the tonalite and the maximum age for the emplacement of the stockwork and disseminated Cu-Zn-Ag mineralization that overprints the tonalite.

Zircon grains in sample 20MDS-186B are also well formed, sharp, and small but are mostly altered, cracked, or broken, clouded, and colorless to brown (Fig. 12E). U-Pb isotope analyses of three, best-quality single grain zircon fractions show a linear array of slightly reverse discordant data, with $^{207}\text{Pb}/^{206}\text{Pb}$ ages between 2694.6 and 2696.0 Ma (Table 1, Fig. 12D). Th/U ratios range from 0.51 to 0.62 and are typical of igneous zircons (Kirkland et al., 2015). A weighted average $^{207}\text{Pb}/^{206}\text{Pb}$ age calculated from all three fractions is 2695.3 \pm 1.0 Ma (MSWD = 1.0; probability of fit = 37%) and represents the crystallization age of the tonalite dike. This also provides a minimum age for the Joliet Cu deposit and a maximum age for overprinting Fe carbonate alteration accompanying intrusion of the late, crosscutting, gold-bearing Vox vein.

Oxygen Isotope Analysis

The histogram of all whole-rock δ^{18} O samples from the mafic and felsic host rocks at the Cu-Zn-Ag occurrences shows a range from 2.9 to 5.9% (mean = $4.8\% \pm 0.6$; Fig. 13A; App. Table A3). These values are on average lower than the background mafic and felsic whole-rock δ^{18} O values within the Powell block from 4.4 to 7.7% (mean = 5.9% ± 1.1 ; Fig. 13A, B; App. Table A3). The background values represent the least altered samples, which were selected from the study area based on petrographic observations (preserved primary textures, minimal modal abundance of alteration minerals) and/or lithogeochemical assessment (Ishikawa alteration index [AI]: AI <65 [mafic], AI <85 [felsic]; App. Fig. A3; Ishikawa et al., 1976). Least altered mafic samples from this study have $\delta^{18}O_{\text{whole-rock}}$ values between 4.4 and 5.4%. Least-altered felsic samples have $\delta^{18}O_{whole-rock}$ values slightly higher than the mafic samples, ranging from 5.5 to 7.7% (Fig. 13). By comparison, a histogram for all whole-rock δ^{18} O samples from the altered host rocks of the gold quartz-carbonate vein deposits illustrate a range from 5.8 to 10.3% (x = 7.7% ± 1.2; Fig. 13A; App. Table A3). These values are on average higher than the background values within the Powell block and the altered wall rocks associated with the Cu-Zn-Ag prospects (Fig. 13A, B).

The alteration surrounding the individual Cu-Zn-Ag occurrences typically extends for a minimum of ~50 to 100 m (Fig. 6); however, collectively these closely spaced occurrences and their associated alterations span an area of ~3.5 km² with $\delta^{18}O_{whole\text{-rock}}$ values dominantly <6% (Fig. 2). Within ~20 to 50 m of the gold quartz-carbonate veins and E-W-striking shear zones the $\delta^{18}O_{whole\text{-rock}}$ values increase by ~2 to 5% (Figs. 2, 10C, D), which if superimposed on previously lower $\delta^{18}O_{whole\text{-rock}}$ chlorite-sericite—altered rocks associated with the Cu-Zn-Ag veins, results in an apparent least altered $\delta^{18}O_{whole\text{-rock}}$ value (~6–8%; Fig. 10D). For example, all the samples collected in proximity to the Powell-Rouyn vein (Fig.

13B; App. Fig. A5) show $\delta^{18}O_{whole-rock}$ values of 6.4 to 7.3%, which fall within the background least altered $\delta^{18}O_{whole-rock}$ values compared to the ~8 to 10% $\delta^{18}O_{whole-rock}$ values found surrounding the Vox and Silidor veins (Fig. 10C, D). The Powell-Rouyn vein is superposed on an area of pervasive chlorite-sericite alteration with $\delta^{18}O_{whole-rock}$ values <6% (Fig. 2).

Six vein quartz samples from the Cu-Zn-Ag veins yielded $\delta^{18}O_{quartz}$ values that range from 6.4 to 9.4% with an average of 8.5 \pm 0.8% (Fig. 13B; App. Table A4). The $\delta^{18}O_{quartz}$ values (n = 5) for quartz in the gold quartz-carbonate veins range from 9.3 to 12.6% with an average value of 11.3 \pm 0.8% (Fig. 13B; App. Table A4). This agrees with the previously reported $\delta^{18}O_{quartz}$ value (n = 6) for the Silidor vein of 10.1 \pm 1.2% (Carrier et al., 2000).

The $\delta^{18}O_{quartz}$ values were used to calculate the isotopic composition of the fluid from which the quartz crystallized and thus interpret potential fluid sources. Using the isotopic fractionation equation between quartz and H₂O from Sharp et al. (2016) with an inferred temperature range of 250° to 350°C, which is typical for VMS systems (e.g., Cathles, 1993; Hannington et al., 2003), the range of $\delta^{18}\bar{O}_{fluid}$ from which the quartz in the Cu-Zn-Ag veins crystallized is -0.4 to 3.1% (Table 2; Fig. 13B; Matsuhisa et al., 1979; Sharp et al., 2016). This is consistent with the reported -2 to $4\% \delta^{18}O_{\text{fluid}}$ range for VMS hydrothermal fluids (Huston, 1999). In contrast, the $\delta^{18}O_{quartz}$ values for the gold quartz-carbonate veins are similar to the typical range for orogenic gold mineralization throughout the Superior Province, which is ~12.5 to 15% δ¹⁸O_{quartz} (McCuaig and Kerrich, 1998; Goldfarb et al., 2005; Quesnel et al, 2023). Using a temperature range of 250° to 350°C, typical for orogenic systems and consistent with the estimated pressure-temperature (P-T) conditions for the Blake River Group in the Rouyn-Noranda area (270°C; Powell et al., 1995), the calculated $\delta^{18}O_{\text{fluid}}$ composition for the gold quartz-carbonate veins is 2.4 to 5.9% (Table 2; Fig. 13B; Matsuhisa et al., 1979; Sharp et al., 2016). This is in agreement with a metamorphic fluid source (Beaudoin and Pitre, 2005; Beaudoin and Chiaradia, 2016; Quesnel et al., 2023), but it also partially overlaps with the estimated ranges for magmatic and Archean seawater fluids (Fig. 13B), which might suggest fluid mixing and involvement of more than one fluid source.

Table 2. Vein Fluid Source Summary

	Quartz-sulfide Cu-Zn-Ag veins	Gold quartz-carbonate veins
Hydrothermal system	Volcanogenic massive sulfide	Orogenic gold
Temperature range	250°–350°C	$250^{\circ} - 350^{\circ} C$
$\delta^{18}O_{quartz}$ values	6.4-9.4	9.3-12.6
Mean δ ¹⁸ O _{quartz} value	8.5	11.3
$\delta^{18} O_{H_2O}$ range calculated from minimum $\delta^{18} O_{quartz}$	–2.5 to 1	0.4–3.9
$\delta^{18}O_{H_2O}$ range calculated from maximum $\delta^{18}O_{quartz}$	0.5–4	3.7–7.2
$\delta^{18}O_{\rm H_2O}$ range calculated from mean $\delta^{18}O_{\rm quartz}$	-0.4 to 3.1	2.4–5.9

Note: stable isotope fractionation factor for Qtz-H $_2$ O system computed using equation from Sharp et al., 2016

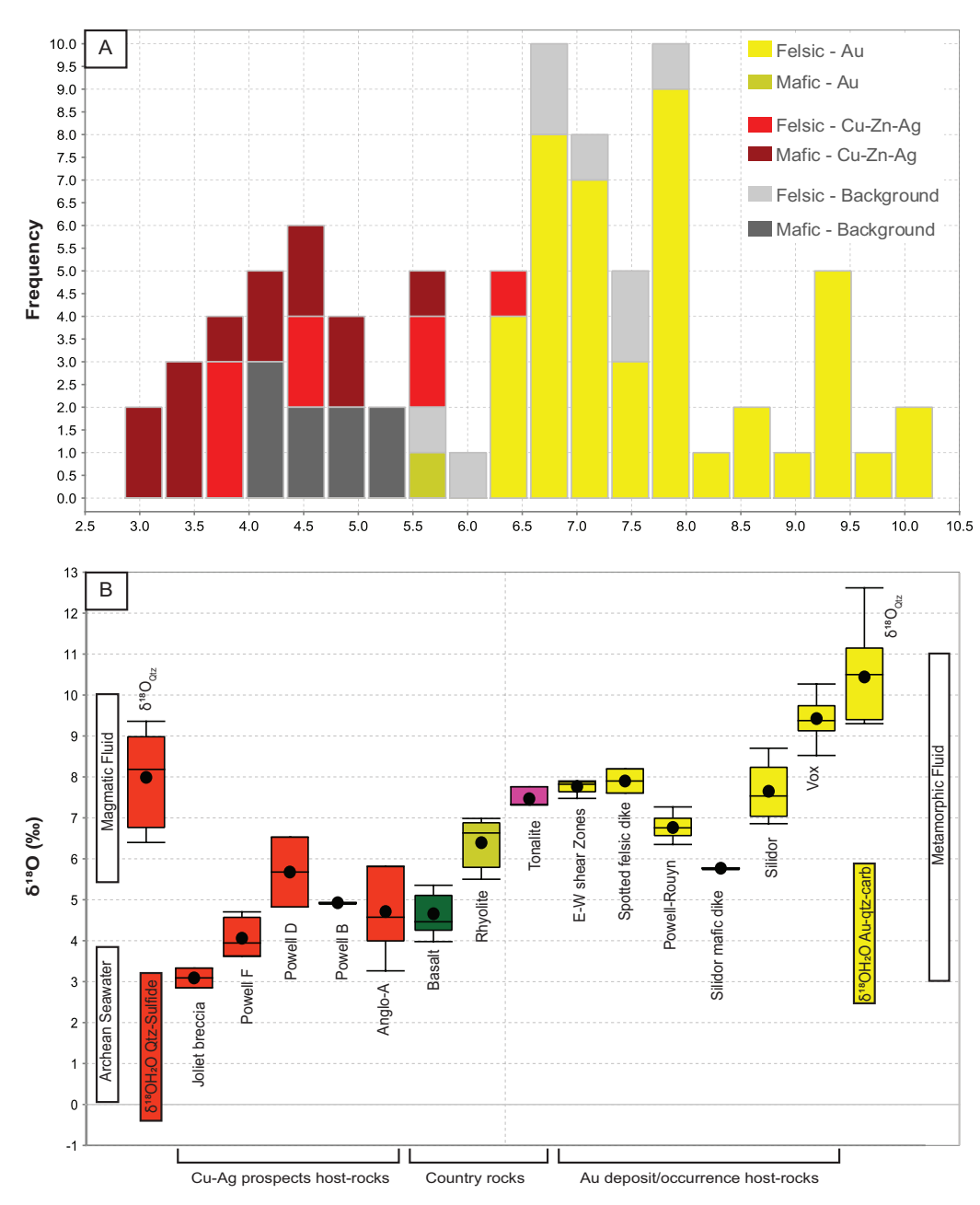


Fig. 13. (A) Histogram of whole-rock $\delta^{18}O$ values for rock types distal to mineralization (gray) and within alteration halos associated with the quartz-sulfide Cu-Zn-Ag veins (red) and gold quartz-carbonate veins (yellow). Data are grouped into 20 bins, 0.371‰ wide. The shades within each group reflect the mafic and felsic composition range. (B) Comparison of whole-rock $\delta^{18}O$ values for altered host rocks associated with Cu-Zn-Ag and Au mineral prospects, occurrences, and deposits with the background country-rock values for the main rock types in the Powell block. Quartz $\delta^{18}O$ values from quartz-sulfide Cu-Zn-Ag veins and gold quartz-carbonate veins are shown on far left and right of the diagram, respectively. The $\delta^{18}O$ values calculated from the mean $\delta^{18}O$ quartz values and estimated temperature range from the two vein types (Table 2) are also plotted in comparison to the range of $\delta^{18}O$ values for the possible fluid sources (Sheppard, 1986; Pope et al., 2012; Johnson and Wing, 2020).

Discussion

Timing of gold quartz-carbonate vein versus quartz-sulfide Cu-Zn-Ag-rich vein mineralization

The different vein sets within the Blake River Group exhibit evidence for distinct superposition of contrasting hydrothermal mineralization styles separated in time. Two lines of field evidence suggest that the Cu-Zn-Ag veins are older than the gold quartz-carbonate veins: (1) the spotted alteration associated with the Cu-Zn-Ag veins overprints the volcanic rocks at the Vox occurrence and is itself overprinted by ankerite proximal to ~E-W-striking brittle-ductile shear zones; and (2) minor quartz-sulfide veins, disseminated sulfides, and alteration associated with Cu-Zn-Ag veins are locally crosscut by quartz-carbonate veins of similar orientation to the main gold quartz-carbonate veins at the Powell F zone. This is further

supported by the new CA-ID-TIMS U-Pb zircon age for the tonalite dike that cuts the Joliet Cu deposit and is also overprinted by the Vox gold quartz-carbonate vein and therefore indicates the minimum age of the Cu mineralization and the maximum age of the Au mineralization at 2695.3 \pm 1.0 Ma. The CA-ID-TIMS U-Pb zircon age of 2697.6 ± 0.7 Ma for the altered Powell D-zone tonalite reported herein is within error of the 2698.0 \pm 0.9 Ma age of an altered tonalite intrusion at the Joliet breccia (Schofield et al., 2021). The two intrusions are similar in age to the upper Blake River Group strata (2699–2695 Ma) and associated VMS hydrothermal system (e.g., Bouchard Hebert VMS deposit, Fig. 1) and suggest that the quartz-sulfide Cu-Zn-Ag-rich vein- and breccia-hosted occurrences were emplaced during the waning stages of volcanic construction of the Blake River Group. In contrast, the gold quartz-carbonate veins were emplaced ~40 to 30 m.y. after the Cu-Zn-Ag veins during the main regional north-south shortening event at ca. 2670 to 2660 Ma (Dubé and Mercier-Langevin, 2020), discussed further below.

Quartz-sulfide Cu-Zn-Ag-rich veins, emplacement, and origin

Quartz-sulfide Cu-Zn-Ag mineralized zones and their associated alteration halos are crosscut by the main E-W-striking S_2 cleavage. This indicates that the veins were emplaced prior to D_2 , either during D_1 or earlier volcanic or magmatic events. The veins are spatially associated with brittle NE-striking structures, which have typically been interpreted as reactivated synvolcanic structures (De Rosen Spence, 1976; Lichtblau and Dimroth, 1980; Dimroth et al., 1982). The northeast structures associated with the Cu-Zn-Ag veins are marked by stratigraphic offsets and contain spherulitic felsic dikes and intrusion-related breccias, consistent with a synvolcanic origin.

The Cu-Zn-Ag veins in the Powell block crosscut older (2703–2701 Ma) Blake River Group strata, as do the Mc-Dougall and C-shaft veins in the Flavrian block and the Joliet breccia in the Powell block (Gibson et al., 1983; Zubowski, 2011; Schofield et al., 2021). The similarities in terms of metal association, textures, paragenesis, and alteration styles between the quartz-sulfide Cu-Zn-Ag-rich veins, the Joliet breccia mineralization, and the McDougall-Despina and Cshaft quartz-sulfide veins (e.g., Zubowski, 2011; Schofield et al., 2021) are consistent with their formation from the same hydrothermal system. The McDougall-Despina and C-shaft quartz-sulfide veins occur along structures that localized magmatic and hydrothermal activity (e.g., Corbet, Millenbach, and Amulet massive sulfide deposits), and the veins are identical to the stockwork veins that immediately underlie and grade into the massive sulfide lenses and thus were interpreted as part of the same VMS-related upflow zone (Knuckey et al., 1982; Gibson et al., 1983; Zubowski, 2011). Although the quartz-sulfide Cu-Zn-Ag-rich vein- and breccia-hosted mineral occurrences in the Powell block do not directly underlie and grade into any known massive sulfide lenses, they are also located along interpreted synvolcanic structures, and occur in the stratigraphic footwall to similar-age volcanic rocks, and are therefore interpreted to be the deep structural roots or upflow zones for a VMS hydrothermal system (Fig. 14A) that may have fed stratigraphically higher and younger VMS

deposits (e.g., Gibson et al., 1983; Cathles, 1993; Zubowski, 2011; Schofield et al., 2021).

However, although mineralogically and chemically the alteration zonation associated with the veins is typical of VMS systems (e.g., Hannington et al., 2003), the spotted texture is peculiar. It resembles dalmatianite (De Rosen-Spence, 1969), a cordierite porphyryoblastic rock associated with VMS deposits in the contact metamorphic aureole of Lac Dufault pluton in the Flavrian block to the north (Fig. 1). Like dalmatianite, the spotted alteration texture developed in altered rocks with a bulk composition reflecting the transition from sericite to chlorite alteration (Franklin et al., 2005; Schofield et al., 2021). However, the spots are texturally distinctive from retrogressed cordierite porphyroblastic dalamatianite alterations. The concentric zoning of the spots is unusual for retrogressed porphyroblasts and suggests a primary metasomatic origin. The albite-rich cores of the spots indicate that the spots may have nucleated on preexisting albite microlites and/or phenocrysts of previously spilitized rock types. The presence of a similar style of spots in chlorite- and sericite-altered rocks at the Corbet VMS deposit (Knuckey and Watkins, 1982), the Joliet breccia (Schofield et al., 2021), and overprinting the number 14 lens of the Millenbach VMS deposit (Fig. 1; Riverin, 1977) implies that this texture is patchily distributed in altered rocks throughout the Noranda Volcanic Complex, but, owing to its close spatial association with ca. 2698 Ma intrusions, it is likely younger than the ca. 2703 to 2701 Ma VMS mineralization.

Gold quartz-carbonate veins, emplacement, and origin

McMurchy (1948) and Carrier et al. (2000) interpreted the gold quartz-carbonate veins in the Noranda camp as late-orogenic deposits emplaced during post- D_2 regional folding and post- D_3 reverse-dextral shearing along major E-W-striking faults. Carrier et al. (2000) suggested that the gold quartz-carbonate veins occupy NW-striking reverse shear zones, which formed during northeast-southwest bulk shortening associated with sinistral reactivation of the major E-W-striking faults (Horne and Beauchastel faults). However, apart from the lack of evidence for sinistral reactivation of the major E-W-striking faults (e.g., Powell fault, Fig. 5) and reverse shearing along the veins exposed at the surface, the veins are folded with the S_2 cleavage axial planar to the folds, so they cannot be late orogenic as proposed by McMurchy (1948) and Carrier et al. (2000).

The gold quartz-carbonate veins vary in orientation along strike, and the poles to individual vein segments define a great circle (Fig. 10E) that is similar in orientation to the great circle defined by the poles to bedding measured in the hinge and limbs of the Powell syncline, indicating that the veins were folded during the deformation event that produced the Powell syncline. The pole to the great circle defined by the folded veins represents the axis of the folds overprinting the veins. It plunges moderately to the east-northeast and lies along the regional S_2 cleavage. This structural relationship, together with the observed overprinting of the vein alteration halos by the cleavage, suggests that the veins were emplaced during D_2 , as were most gold deposits in the southern Abitibi greenstone belt (Dubé and Mercier-Langevin, 2020), including the nearby Donalda deposit (Riverin et al., 1990; Robert et al.,

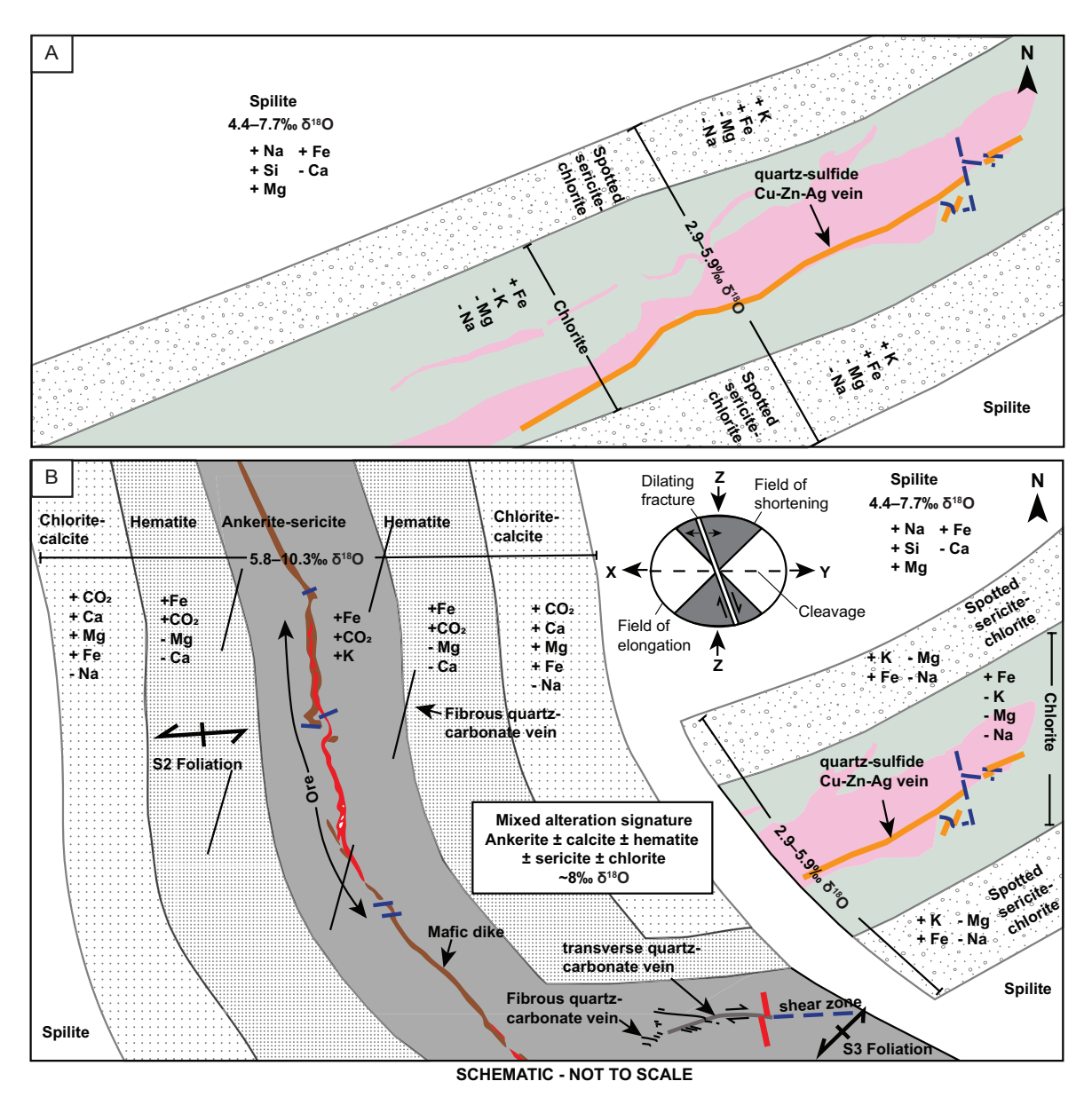


Fig. 14. Schematic diagram illustrating the relative timing and general morphology of the quartz-sulfide Cu-Zn-Ag-rich (A) and gold quartz-carbonate (B) vein types, using the Powell F-zone and Powell-Rouyn (1,550' level from McMurchy, 1948) vein traces for reference. The mineralogical, chemical, and isotopic changes associated with their alteration envelopes are shown schematically, along with the mixed alteration signal within their overlap zone. The strain ellipse during D2 is shown with the orientation of preexisting fractures that are expected to dilate. Note that a component of dextral shear is also permissible along a NNW-oriented structure.

1996). The north-northwest strike of the veins is largely controlled by the mechanical anisotropies created by rheological contrasts between the mafic dikes and host tonalite (e.g., Belkabir et al., 1993; Blenkinsop et al., 2020). Because the strike of the mafic dikes is within ~20° of the north-south bulk shortening direction during the D_2 event (Fig. 14B), the diketonalite contacts acted as planes of weakness that underwent a dextral shear traction as they opened up parallel to the bulk extension direction (e.g., Sibson, 2001; Lafrance, 2004). Goldbearing hydrothermal fluids flowed into the newly created NNW-striking fractures and deposited quartz veins (Silidor), and where offset markers are present (Vox vein), displaced those markers in a dextral manner.

 $Comparison\ of\ alteration\ signatures\ associated\ with\ both\ vein\ systems$

There is a strong lithological control on the alteration mineralogy associated with the gold quartz-carbonate veins, with the requirement of primary ferromagnesian minerals in the host rock in order to form hydrothermal ankerite. Within felsic-dominated successions, this results in cryptic alteration signatures that are similar to regional synvolcanic spilitic alteration. In contrast, the quartz-sulfide Cu-Zn-Ag-rich veins exhibit consistent alteration mineralogy that is controlled by primary permeability regardless of initial host-rock composition. Both hydrothermal systems introduce chlorite into the mineral assemblage and have distinguishable compositional differences

(Fig. 9). Likewise, these two hydrothermal systems have contrasting effects on whole-rock $\delta^{18}\text{O}$ values.

Whole-rock δ^{18} O values ultimately depend on the oxygen isotope composition of the constituent minerals and the modal mineralogy of the rock, thus composition in part controls the whole-rock $\delta^{18}O$ values. For example, pristine rhyolite typically has a whole-rock δ^{18} O value ~2% higher than its mafic counterparts (Beaudoin et al., 2014). Hydrothermal alteration modifies the oxygen isotope composition of fresh rocks because of the formation of new minerals at the expense of primary minerals (Muehlenbachs, 1986). Altered mafic and felsic samples that are spatially associated with the Cu-Zn-Ag prospects and Au occurrences display lower and higher whole-rock δ^{18} O values, respectively, relative to the background values of their least altered precursors (Fig. 13A, B). The difference in whole-rock δ^{18} O values for altered rocks associated with both types of veins could be controlled by different fluid sources, temperatures of alteration, or fluid/rock

Chlorite and sericite mineral assemblages and isotopically light whole-rock δ^{18} O values of 2.9 to 5.9% within the altered rocks adjacent to the Cu-Zn-Ag occurrences are consistent with hydrothermal alteration driven by modified Archean seawater (Fig. 13C; Pope et al., 2012; Johnson and Wing, 2020). In contrast, the gold quartz-carbonate veins are characterized by relatively isotopically heavy whole-rock δ^{18} O values of 5.8 to 10.3% and carbonate (ankerite ± calcite), albite, sericite, fuchsite, hematite, and chlorite mineral associations, which is consistent with hydrothermal alteration driven by interaction with a metamorphic fluid (Fig. 13C; Sheppard, 1986), possibly mixed with a lower $\delta^{18}O$ upper crustal fluid, such as Archean seawater, trapped as fluid inclusions in the volcanic rocks (e.g., quartz-filled vesicles; Fig. 13C). Mixing between these two fluid types was also invoked for the Val d'Or district, 100 km to the east (Beaudoin and Pitre, 2005) and for quartztourmaline-carbonate veins along the Larder Lake Cadillac fault within the Rouyn-Noranda mining district (Raymond, 2022). Likewise, despite the similarities in textures of quartz within the gold quartz-carbonate and Cu-Zn-Ag veins, quartz from the two vein sets can be clearly distinguished by different $\delta^{18}O_{quartz}$ values, which are relatively higher for the gold quartz-carbonate veins at an average of 11.3 ± 0.8% compared to an average of $8.5 \pm 0.8\%$ for the Cu-Zn-Ag veins (Fig. 13B). This is consistent with different fluid sources for the two vein systems and associated alteration (Fig. 13B; Table 2).

Significance of the superposition of alteration events on the district-scale alteration patterns

In a landmark study, Cathles (1993) used whole-rock oxygen isotope data to distinguish district-scale, higher-temperature, VMS chlorite- and sericite-altered upflow zones characterized by whole-rock δ^{18} O values <6% from lower-temperature, albite-, epidote-, carbonate-, and/or quartz-altered downflow zones characterized by whole-rock δ^{18} O values of 8.5 to 14%. Cathles (1993) interpreted rocks with whole-rock δ^{18} O values between 6 and 8% as unaltered. Taylor et al. (2014) refined the pattern of oxygen isotope anomalies in the Powell block and, along with Cathles (1993) and Hannington et al. (2003), interpreted the extensive areas of sericite-quartz alteration

and whole-rock δ^{18} O values of 8.5 to 14‰ associated with the Horne and Quemont deposits in terms of semiconformable synvolcanic downflow zones owing to seawater recharge. It was proposed that this anomalously high whole-rock δ^{18} O alteration signature for the Horne and Quemont deposits located stratigraphically above lower whole-rock δ^{18} O alteration signatures defined by MacLean and Hoy (1991) might be a useful exploration vector specifically for large and Au-rich VMS deposits (Cathles, 1993). However, in all these studies the effect of an orogenic gold system superimposed upon a VMS system either was not considered or was assumed to have had a negligible effect (e.g., Maclean and Hoy, 1991; Taylor et al., 2014). As such, it is noteworthy that there is considerable overlap between the documented range of whole-rock δ^{18} O values associated with orogenic systems (e.g., McCuaig and Kerrich, 1998; Beaudoin, 2011) and seawater recharge zones associated with VMS deposits (e.g., Cathles, 1993; Taylor et al., 2014).

This study shows that alteration of the host volcanic rocks during the Cu-Zn-Ag vein-forming event lowered their wholerock δ^{18} O values to 2.9 to 7.7% (Fig. 14A), but subsequent overprinting alteration associated with the later gold quartzcarbonate veins locally increased their whole-rock $\delta^{18}O$ values to ~5.8 to 10.3% (Fig. 14B). Thus, the whole-rock δ^{18} O values in the Powell block are dominantly related to the alteration signatures associated with one of the two younger vein mineralization events and locally represent averages of two or more alteration events (Fig. 14B). In addition, many of the interpreted VMS-related downflow zones, delineated by relatively enriched whole-rock δ^{18} O values, overlap with known orogenic deposits and major structures such as the Horne Creek fault and Larder Lake Cadillac Break, which are known to have localized orogenic ore-forming fluids (e.g., Riverin et al., 1990; Robert et al., 1996; Dubé and Mercier-Langevin, 2020). Likewise, this study has demonstrated that the juxtaposition of orogenic-related albite ± ankerite ± calcite ± sericite alteration on VMS and/or magmatic-hydrothermal-related chlorite-sericite alteration can produce lower whole-rock δ^{18} O values than what might be expected for typical orogenic deposits and may result in the misinterpretation that such rocks are unaltered. This has been problematic for the use of whole-rock δ^{18} O values to discern VMS alteration patterns in the Powell block. For example, Taylor et al. (2014) did not detect distinct zones of VMS-related alteration in the footwall to the Quemont VMS deposit in part because the superposition of orogenic gold alteration on VMS-altered rocks effectively masked the early VMS alteration and led to interpretations that the rocks were unaltered. The intense quartz-sericite alteration surrounding the Horne and Quemont VMS deposits, characterized by anomalously high whole-rock δ^{18} O values of 6.6 to 11.6% (MacLean and Hoy, 1991; Taylor et al., 2014) overlaps with the 5.8 to 10.3% $\delta^{18}O_{whole-rock}$ range associated with the orogenic overprint documented throughout the Powell block in this study. Both deposits occur proximal to the Horne Creek fault (Fig. 1), and Krushnisky (2018) described a 10-m-wide fault zone associated with intense sericite, hematite, and Fe-carbonate alteration crosscutting the Horne mineralization, which is consistent with an orogenic gold alteration overprint. The results here illustrate that in complex metallogenic environments with multiple overprinting hydro-

thermal alteration types, care must be taken in interpreting whole-rock δ^{18} O values and it must be integrated with field observations, crosscutting relationships, and petrography.

Conclusions

The Powell block of the Rouyn-Noranda mining district contains two types of epigenetic quartz veins: quartz-sulfide Cu-Zn-Ag-rich veins and gold quartz-carbonate veins. Field relationships suggest that the Cu-Zn-Ag veins formed earlier than the gold quartz-carbonate veins and that the two are genetically unrelated. This is further supported by the contrasting alteration mineral associations, lithogeochemical and isotopic alteration signatures, and metal tenors and $\delta^{18}O_{quartz}$ values for both vein styles (11.3 \pm 0.8% for the Au veins and 8.5 ± 0.8% for the Cu-Zn-Ag veins), which indicate that different fluid sources are likely for the two vein systems. Assuming a temperature range of 250° to 350°C, which is typical for VMS systems, the range of $\delta^{18}O_{fluid}$ from which the quartz in the Cu-Zn-Ag veins crystallized is -0.4 to 3.1‰. In contrast, using the same temperature range, which is also common in orogenic systems, the calculated $\delta^{18}O_{\text{fluid}}$ composition for the gold quartz-carbonate veins is 2.4 to 5.9%. In addition, new CA-ID-TIMS U-Pb zircon ages for two tonalite intrusions constrain the maximum age for the Cu mineralization to $2697.6 \pm 0.7 \text{ Ma}$, and the minimum age to $2695.3 \pm 1.0 \text{ Ma}$; the younger age also defines a maximum age for emplacement of the gold quartz-carbonate veins.

Despite the different timing for the formation of the two vein systems, in both cases preexisting structures controlled the hydrothermal fluid flow and ultimately dictated the orientation of the resulting hydrothermal veins and their subsequent deformation style. Éarly ENE-striking Cu-Zn-Ag veins may have utilized preexisting structures marked by older (ca. 2703-2701 Ma) Blake River Group felsic dikes, but clearly were emplaced during a younger ca. 2698 Ma Blake River Group magmatic-hydrothermal event. The veins may represent a relatively deeper manifestation of a ca. 2699 to 2695 Ma VMS system that formed in rocks at a higher stratigraphic level. In contrast, the gold quartz-carbonate veins were emplaced along preexisting mechanical anisotropies created by NNW-striking mafic dikes ~30 to 40 m.y. after the Cu-Zn-Ag veins during early D₂ north-south shortening at ca. 2670 to 2660 Ma.

Both vein sets are associated with fracture-controlled to pervasive hydrothermal alteration, which overprints rocks that were subject to early sea floor spilitization. Thus, superposition of at least three independent types of alteration is observed within the Powell block and in the larger Rouyn-Noranda mining district: (1) early quartz-albite (spilitization); (2) chlorite and spotted sericite-chlorite alteration characterized by Fe-rich chlorite and whole-rock δ^{18} O values of 2.9 to 5.9%; and (3) carbonate, sericite, chlorite, and hematite alteration characterized by Mg-rich chlorite and whole-rock δ^{18} O values of 5.8 to 10.3% (Fig. 14). Moreover, where the carbonate alteration associated with the gold quartz-carbonate veins and shear zones is superimposed on the chlorite and spotted sericite-chlorite alteration associated with the Cu veins, an increase of ~2 to 5% whole-rock δ^{18} O values occurs. The whole-rock $\delta^{18}O$ values from samples that have experienced more than one hydrothermal alteration event are thus

an average of the individual signatures, and this juxtaposition of orogenic-related alteration on VMS and/or magmatic-hydrothermal-related alteration can produce lower whole-rock δ^{18} O values than what might be expected for typical orogenic deposits and result in the misinterpretation of such rocks as either unaltered or altered by VMS-related downflow zones. This is problematic for the use of whole-rock δ^{18} O values to discern regional-scale alteration patterns for VMS deposits within any area that has multiple superposed mineralization events. Since superposed mineralization events are ubiquitous in ancient volcanic districts, whole-rock δ^{18} O values should not be used as a stand-alone method to provide vectors to mineralization, particularly at the greenfield exploration stage. The results of this study provide a guide for using a combination of detailed field observations including overprinting relationships between veins, their associated alteration assemblages, and regional structural fabrics, as well as geochronology and mineral and isotopic chemistry, to help decipher and vector within volcanic rocks that are modified by superimposed hydrothermal events.

Acknowledgments

The authors extend much appreciation to Kevin Ansdell, Brian McNulty, and Steve Piercey for their expertise and insight, which greatly improved the manuscript. Thank you also to Sylvain Picard for providing access to historical samples and data for the Silidor deposit. Gérald Riverin and Jean Goutier are also thanked for providing critical historical data. Taus Jørgensen is thanked for helpful discussions and providing invaluable logistical assistance during field work. Field assistants Brittany Courchesne, David Dickson, and Michael Langa are thanked for eager, competent, and able assistance in the field. Yorbeau Resources Inc. is thanked for allowing the use of their rock saw facilities during the field season. Financial support was provided by Metal Earth though a Canada First Research Excellence Fund (CFREF) grant, which comprises a tri-agency initiative of the Natural Sciences and Engineering Research Council (NSERC), Social Sciences and Humanities Research Council (SSHRC), and the Canadian Institutes of Health Research (CIHR). Funding was also provided by federal, provincial, and industry partners of the Mineral Exploration Research Centre (MERC; http://merc.laurentian. ca/research/metal-earth/). This publication is a Metal Earth contribution MERC-ME-2021-68.

REFERENCES

Allmendinger, R.W., Cardozo, N., and Fisher, D., 2012, Structural geology algorithms: Vectors and tensors: Cambridge University Press, Cambridge, 302 p.

Beaudoin, G., 2011, The stable isotope geochemistry of orogenic gold deposits, in Barra, F., Reich, M., Campos, E., and Tornos, F., eds., Biennial Society for Geology Applied to Mineral Deposits (SGA) Meeting, 11th, Antogfagasta, Chile, 2011, Proceedings, p. 556–558.

Beaudoin, G., and Chiaradia, M., 2016, Fluid mixing in orogenic gold deposits: Evidence from the H-O-Sr isotope composition of the Val d'Or vein field (Abitbi, Canada): Chemical Geology, v. 437, p. 7–18.

Beaudoin, G., and Pitre, D., 2005. Stable isotope geochemistry of the Archean Val-d'Or (Canada) orogenic gold vein field: Mineralium Deposita, v. 40, p. 59-75.

Beaudoin, G., Mercier-Langevin, P., Dubé, B., and Taylor, B.E., 2014, Low-temperature alteration at the world-class La Ronde Penna Archean Au-rich volcanogenic massive sulfide deposit, Abitibi subprovince, Quebec, Canada: Evidence from whole-rock oxygen isotopes: Economic Geology, v. 109, p. 167–182.

- Bedeaux, P., Pilote, P., Daigneault, R., and Rafini, S., 2017, Synthesis of the structural evolution and associated gold mineralization of the Cadillac fault, Abitibi, Canada: Ore Geology Reviews, v. 82, p. 49–69.
- Belkabir, A., Robert, F., Vu, L., and Hubert, C., 1993, The influence of dikes on auriferous shear zone development within granitoid intrusions: The Bourlamaque pluton, Val-d'Or district, Abitbi greenstone belt: Canadian Journal of Earth Sciences, v. 30, p. 1924–1933.
- Bleeker, W., 2012, Targeted geoscience initiative 4. Lode gold deposits in ancient deformed and metamorphosed terranes: The role of extension in the formation of Timiskaming basins and large gold deposits, Abitibi greenstone belt—a discussion: Ontario Geological Survey Open File Report 6280, p. 47-1–47-12.
- Blenkinsop, T.G., Oliver, N.H.S., Dirks, P.G.H.M., Nugus, M., Tripp, G., and Sanislav, I., 2020, Structural geology applied to the evaluation of hydrothermal gold deposits: Reviews in Economic Geology, v 21, p. 1–23.
- Blundell, D.J., 2002, The timing and location of major ore deposits in an evolving orogen: The geodynamic context: Geological Society of London, Special Publication 204, p. 1–12, doi: 10.1144/gsl.sp.2002.204.01.01.
- Carrier, A., Jébrak, M., Angelier, J., and Holyland, P., 2000, The Silidor deposit, Rouyn-Noranda district, Abitibi belt: Geology, structural evolution, and paleostress modeling of an Au quartz vein-type deposit in an Archean trondhjemite: Economic Geology, v. 95, p. 1049–1065.
- Cathles, L.M., 1993, Oxygen isotope alteration in the Noranda mining district, Abitibi greenstone belt, Québec: Economic Geology, v. 88, p. 1483–1511.
- Cooke, H.C., James, W.F., and Mawdsley, J.B., 1931, Geology and ore deposits of Rouyn-Harricanaw region, Quebec: Geological Survey of Canada, Memoir 166, 314 p.
- Daigneault, R., Mueller, W.U., and Chown, E.H., 2002, Oblique Archean subduction: Accretion and exhumation of an oceanic arc during dextral transpression, southern volcanic zone, Abitibi subprovince Canada: Precambrian Research, v. 115, p. 261–290.
- De Rosen-Spence, A., 1969, Genèse des roches à cordierite-anthophyllite des gisements cupro-zincifères de la région de Rouyn-Noranda, Québec, Canada: Canadian Journal of Earth Sciences, v. 6, p. 1339–1345.
- De Rosen Spence, A.F., 1976, Stratigraphy, development and petrogenesis of the central Noranda volcanic pile, Noranda, Québec: Ph.D. thesis, Toronto, Ontario, Canada, University of Toronto, 308 p.
- Dimroth, E., Imreh, L., Rocheleau, M., and Goulet, N., 1982, Evolution of the south-central part of the Archean Abitibi belt, Québec, Part I: Stratigraphy and paleogeographic model: Canadian Journal of Earth Sciences, v. 19, p. 1729–1758.
- Dimroth, E., Imreh, L., Goulet, N., and Rocheleau, M., 1983, Evolution of the south-central segment of the Archean Abitibi belt, Québec, Part II: Tectonic evolution and geomechanical model: Canadian Journal of Earth Sciences, v. 20, p. 1355–1373.
- Dubé, B., and Mercier-Langevin, P., 2020, Gold deposits of the Archean Abitibi greenstone belt, Canada: Society of Economic Geologists, Special Publication 23, p. 669–708.
- Fitchett, C., 2012, Metamorphic phase equilibria of hydrothermally altered rocks, Noranda district, Abitibi subprovince, Québec: M.Sc. thesis, Sudbury, Ontario, Canada, Laurentian University, 148 p.
- Franklin, J.M., Sangster, D.M., and Lydon, J.W., 1981, Volcanic-associated massive sulfide deposits: Economic Geology 75th Anniversary Volume, p. 485–627.
- Franklin, J.M., Gibson, H.L., Jonasson, I.R., and Galley, A.G., 2005, Volcanogenic massive sulfide deposits: Economic Geology 100th Anniversary Volume, p. 523–560.
- Galley, A.G., and van Breemen, O., 2002, Timing of synvolcanic magmatism in relation to base-metal mineralization, Rouyn-Noranda, Abitibi volcanic belt, Québec: Geological Survey of Canada, Current Research 2002-F8, p. 1–9.
- Gibson, H.L. and Galley, A.G., 2007, Volcanogenic massive sulphide deposits of the Archean, Noranda District, Quebec: Geological Association of Canada, Mineral Deposits Division, Special Publication 5, p. 533–552.
- Gibson, H.L., Watkinson, D.H., and Comba, C.D.A., 1983, Silicification: Hydrothermal alteration in an Archean geothermal system within the Amulet rhyolite formation, Noranda, Quebec: Economic Geology, v. 78, p. 954–971.
- Goldfarb, R.J., Baker, T., Dubé, B., Groves, D.I., Hart, C.J.R., and Gosselin, P., 2005, Distribution, character, and genesis of gold deposits in metamorphic terranes: Economic Geology 100th Anniversary Volume, p. 407–450.
- Goldie, R., 1976, The Flavrian and Powell plutons, Noranda area, Québec: A geological investigation of the Flavrian and Powell plutons and their relationships to other rocks and structures of the Noranda area: Ph.D. thesis, Kingston, Ontario, Canada, Queen's University, 381 p.

- Goldie, R., Kotila, B., and Seward, D., 1979, The Don Rouyn mine: An Archean porphyry copper deposit near Noranda, Quebec: Economic Geology, v. 74, p. 1680–1684.
- Goulet, N., 1978, Stratigraphy and structural relationships across the Cadillac-Larder Lake fault, Rouyn-Beauchastel area, Quebec: Ph.D. thesis, Kingston, Ontario, Canada, Queen's University, 141 p.
- Guha, J., Archambault, G., and Leroy, J., 1983, A correlation between the evolution of mineralizing fluids and the geomechanical development of a shear zone as illustrated by the Henderson 2 Mine, Quebec: Economic Geology, v. 78, p. 1605–1618.
- Hall, B.V., 1982, Geochemistry of the alteration pipe at the Amulet Upper A deposit, Noranda, Québec: Canadian Journal of Earth Sciences, v. 19, p. 2060–2084.
- Hannington, M.D., Poulsen, K.H., Thompson, J.F.H., and Sillitoe, R.H., 1999, Volcanogenic gold in the massive sulfide environment: Reviews in Economic Geology, v. 8, p. 325–356.
- Hannington, M.D., Santaguida, F., Kjarsgaard, I.M., and Cathles, L.M., 2003, Regional-scale hydrothermal alteration in the Central Blake River Group, western Abitibi subprovince, Canada: Implications for VMS prospectivity: Mineralium Deposita, v. 38, p. 393–422.
- Hey, M.H., 1954, A new review of the chlorites: The Mineralogical Magazine and Journal of The Mineralogical Society, v. 30, p. 277–292.
- Hitzman, M.W., 1999, Routine staining of drill core to determine carbonate mineralogy and distinguish carbonate alteration textures: Mineralium Deposita, v. 34, p. 794–798.
- Hubert, C., Trudel, P., and Gélinas, L., 1984, Archean wrench fault tectonics and structural evolution of the Blake River Group, Abitibi belt, Québec: Canadian Journal of Earth Sciences, v. 21, p. 1024–1032.
- Hughes, C.J., 1973, Late Precambrian volcanic rocks of Avalon, Newfound-land—a spilite/keratophyre province: Recognition and implications: Canadian Journal of Earth Sciences, v. 10, p. 272–282.
- Huston, D.L., 1997, Stable isotopes and their significance for understanding the genesis of volcanic-hosted massive sulfide deposits: A review: Reviews in Economic Geology, v. 8, p. 157–178.
- Hutchinson, R.W., 1987, Metallogeny of Precambrian gold deposits: Space and time relationships: Economic Geology, v. 82, 1993–2007.
- Ishikawa, Y., Sawaguchi, T., Iwaya, S., and Horiuchi, M., 1976, Delineation of prospecting targets for Kuroko deposits based on modes of volcanism of underlying dacite and alteration halos: Mining Geology, v. 26, p. 105–117.
- Ispolatov, V., Lafrance, B., Dubé, B., Creaser, R., and Hamilton, M., 2008, Geologic and structural setting of gold mineralization in the Kirkland Lake-Larder Lake gold belt, Ontario: Economic Geology, v. 103, p. 1309–1340.
- Jaffey, A.H., Flynn, K.F., Glendenin, L.E., Bentley, W.C., and Essling, A.M., 1971, Precision measurement of half-lives and specific activities of ²³⁵U and ²³⁸U: Physical Review, v. 4, p. 1889–1906.
- Jebrak, M., Harnois, L., Carrier, A., and Lafrance, J., 1997, The Don Rouyn-Cu-Au porphyry system, in Couture, J.F., and Robert, F., eds., Atypical gold deposits in the Abitibi belt: Geological Association of Canada, Field Trip B5 guide, Ottawa, 1997, p. 72–78.
- Johnson, B.W., and Wing, B.A., 2020, Limited Archean continental emergence reflected in an early Archean ¹⁸O-enriched ocean: Nature Geoscience, v. 13, p. 243–248.
- Kennedy, L.P., 1985, The geology and geochemistry of the Archean Flavrian pluton, Noranda, Québec: Ph.D. thesis, London, Ontario, Canada, University of Western Ontario, 468 p.
- Kerrich, R., and Kyser, T.K., 1994, 100 Ma timing paradox of Archean gold, Abitibi greenstone-belt (Canada)—new evidence from U-Pb and Pb-Pb evaporation ages of hydrothermal zircons: Geology, v. 22, p. 1131–1134.
- Kirkham, R.V., 1972, Geology of copper and molybdenum deposits: Report of Activities, Part A: Geological Survey of Canada, Paper 72-1A, p. 82–87.
- Kirkland, C.L., Smithies, R.H., Taylor, R.J.M., Evans, N., and McDonald, B., 2015, Zircon Th/U ratios in magmatic environs: Lithos, v. 212, p. 397–414.
- Knuckey, M.J., and Watkins, J.J., 1982, The geology of the Corbet massive sulphide deposit Noranda district, Québec, Canada: Geological Association of Canada, Special Paper 25, p. 297–317.
- Knuckey, M.J., Comba, C.D.A., and Riverin, G., 1982, Structure, metal zoning and alteration at the millenbach deposit, Noranda, Quebec: Geological Association of Canada, Special Paper 25, p. 255–295.
- Kotila, B.W., 1975, An Archean porphyry copper deposit: The Don Rouyn mine, Noranda, Québec, Kingston, Ontario: B.Sc. thesis, Kingston, Ontario, Canada, Queen's University, 21 p.

- Krushnisky, A., 2018, Controls on gold enrichment at the Horne 5 Archean VMS deposit, Abitibi greenstone belt, Québec: M.Sc. thesis, Québec, Canada, Université du Québec, Institute National de la Recherché Scientifique, 238 p.
- Lafrance, B., 2004, Conjugate oblique-extension veins in shear and tensile fracture systems at the Komis gold mine and Mufferaw gold prospect, Northern Saskatchewan: Exploration and Mining Geology, v. 13, p. 129–137.
- Leclerc, F., Harris, L.B., Bédard, J.H., Breemen, O.V., and Goulet, N., 2012, Structural and stratigraphic controls on magmatic, volcanogenic, and shear zone-hosted mineralization in the Chapais-Chibougamau mining camp, northeastern Abitibi, Canada: Economic Geology, v. 107, p. 963–989.
- L'Heureux, M., 1992, Caractérisation géochimique des volcanites et d'une cheminée d'altération dans la partie oust du bloc de Powell, Rouyn-Noranda, Québec: M.Sc. thesis, Québec, Canada, L'Université du Québec a Chicoutimi, 116 p.
- Lichtblau, A., and Dimroth, E., 1980, Stratigraphy and facies at the south margin of the Archean Noranda Caldera, Noranda, Québec: Geological Survey of Canada, Current Research Part A, p. 69–76.
- Maclean, W.H., and Hoy, L.D.,1991, Geochemistry of hydrothermally altered rocks at the Horne mine, Noranda, Quebec; Economic Geology, v. 86, p. 506–528.
- Matsuhisa, Y., Goldsmith, J.R., and Clayton, R.N., 1979, Oxygen isotopic fractionation in the system quartz-albite-anorthite-water: Geochimica et Cosmochimica Acta, v. 43, p. 1131–1140.
- McCuaig, T.C., and Kerrich, R., 1998, P-T-t-deformation-fluid characteristics of lode gold deposits: Evidence from alteration systematics: Ore Geology Reviews, v. 12, p. 381–453.
- McMurchy, R.C., 1948, Powell-Rouyn mine, in Structural geology of Canadian ore deposits: Montreal, Canadian Institute of Mining and Metallurgy, Mercury Press Ltd., p. 739–747.
- McNicoll, V., Goutier, J., Dubé, B., Mercier-Langevin, P., Ross, P.-S., Dion, C., Monecke, T., Legault, M., Percival, J., and Gibson, H., 2014, U-Pb geochronology of the Blake River Group, Abitibi greenstone belt, Quebec, and implications for base metal exploration: Economic Geology, v. 109, p. 27–59, doi: 10.2113/econgeo.109.1.27.
- Mortensen, J.K., 1993, U-Pb geochronology of the eastern Abitibi subprovince: Part 2: Noranda-Kirkland Lake area: Canadian Journal of Earth Sciences, v. 30, p. 29–41.
- Muehlenbachs, K., 1986, Alteration of the oceanic crust and the ¹⁸O history of seawater: Reviews in Mineralogy, v. 16, p. 425–444.
- Piette-Lauzière, N., Guillmette, C., Bouvier, A., Perrouty, S., Pilote, P., Gaillard, N., Lypaczewski, P., Linnen, R.L., and Olivo, G.R., 2019, The timing of prograde metamorphism in the Pontiac subprovince, Superior craton; implications for Archean geodynamics and gold mineralization: Precambrian Research, v. 320, p. 111–136.
- Pilote, P., Robert, F., Sinclair, W.D., Kirkham, R.V., and Daigneault, R., 1995, Porphyry-type mineralization in the Doré Lake Complex: Clark Lake and Merrill Island area: Geological Survey of Canada, Open File 3143, p. 65–86.
- Pope, E.C., Bird, D.K., and Rosing, M.T., 2012, Isotope composition and volume of Earth's early oceans: Proceedings of the National Academy of Sciences, v. 109, p. 4371–4376.
- Poulsen, K.H., 2017, The Larder Lake-Cadillac Break and its gold districts: Reviews in Economic Geology, v. 19, p. 133–167.
- Powell, W.G., Carmichael, D.M., and Hodgson, C.J., 1995, Conditions and timing of metamorphism in the southern Abitibi greenstone belt, Québec: Canadian Journal of Earth Sciences, v. 32, p. 787–805, doi: 10.1139/
- Quesnel, B., Scheffer, C., and Beaudoin, G., 2023, The light stable isotope (hydrogen, boron, carbon, nitrogen oxygen, silicon, sulfur) composition of orogenic gold deposits, in Huston, D., and Gutzmer, J., eds., Isotopes in economic geology, metallogenesis and exploration: Society for Geology Applied to Mineral Deposits (SGA), Special Publication, p. 283–328.
- Raymond, G., 2022, Variation spatiale des conditions de circulation des fluides à l'origine de la minéralisation en or orogénique dans le segment Augmitto-Bouzan (sous-province de l'Abitibi, Québec, Canada): M.Sc. thesis, Québec City, Québec, Université Laval, 107 p.
 Riverin, G., 1977, Wall-rock alteration at the Millenbach mine, Noranda,
- Riverin, G., 1977, Wall-rock alteration at the Millenbach mine, Noranda, Québec: Ph.D. thesis, Kingston, Ontario, Queen's University, 255 p.

- Riverin, G., Bernard, D., and Boily, B., 1990, The Donalda gold deposit, Rouyn-Noranda, Québec, in Rive, M., Verpaelst, P., Gagnon, Y., Lulin, J.M., Riverin, G., and Simard, A., eds., The Northwestern Québec polymetallic belt: Canadian Institute of Mining and Metallurgy, Special Volume 43, p. 199–209.
- Robert, F., and Poulsen, K.H., 2001, Vein formation and deformation in greenstone gold deposits: Reviews in Economic Geology, v. 14, p. 111–155.
- Robert, F., Boullier, A.-M., and Firdaous, K., 1996, Geometric aspects of a large extensional vein, Donalda deposit, Rouyn-Noranda, Québec: Geological Survey of Canada, Current Research 1996-C Canadian Shield, p. 147–155.
- Robert, F., Poulsen, K.H., Cassidy, K.F., and Hodgson, C.J., 2005, Gold metallogeny of the Superior and Yilgarn cratons: Economic Geology 100th Anniversary Volume, p. 1001–1033.
- Sawkins, F.J., 1990, Metal deposits in relation to plate tectonics, 2nd ed.: Springer-Verlag, 475 p.
- Schofield, M., Gibson, H., Lafrance, B., Poulsen, K.H., Marsh, J., Hamilton, M.A., and Jørgensen, T.R.C., 2021, Recognizing subsurface breccias in Archean terranes: Implications for district scale metallogeny: Precambrian Research, v. 361, article 106264.
- Scott, S.D., 1980, Geology and structural control of Kuroko-type massive sulphide deposits: Geological Association of Canada, Special Paper 20, p. 705–721
- Setterfield, T.N., Hodder, R.W., Gibson, H.L., and Watkins, J.J., 1995, The McDougall-Despina fault set, Noranda, Québec: Evidence for fault-controlled volcanism and hydrothermal fluid flow: Exploration and Mining Geology, v. 4, p. 381–393.
- Sharp, Z.D., Gibbons, J.A., Maltsev, O., Atudorei, V., Pack, A., Sengupta, S., Shock, E.L., and Knauth, L.P., 2016, A calibration of the triple oxygen isotope fractionation in the SiO₂-H₂O system and applications to natural samples: Geochimica et Cosmochimica Acta, v. 186, p. 105–119.
- Sheppard, S.M.F., 1986, Characterization and isotopic variations in natural waters: Reviews in Mineralogy and Geochemistry, v. 16, p. 165–183.
- Sibson, R.H., 2001, Seismogenic framework for hydrothermal transport and ore deposition: Reviews in Economic Geology, v. 14, p. 25–50.
- Sillitoe, R.H., 1978, Metallogenic evolution of a collisional mountain belt in Pakistan: A preliminary analysis: Geological Society of London Journal, v. 135, p. 377–387.
- Taylor, B.E., De Kemp, E., Grunsky, E., Martin, L., Maxwell, G., Rigg, D., Goutier, J., Lauzière, K., and Dubé, B., 2014, Three-dimensional visualization of the Archean Horne and Quemont Au-bearing volcanogenic massive sulfide hydrothermal systems, Blake River Group, Quebec: Economic Geology, v. 109, p. 183–203.
- Tripp, G.T., Tosdal, R.M., Blenkinsop, T., Rogers, J.R., and Halley, S., 2020, Neoarchean eastern goldfields of Western Australia, in Sillitoe, R.H., Goldfard, R.J., Robert, F., and Simmons, S.F., eds.: Geology of the World's Major Gold Deposits and Provinces: Society of Economic Geologists, Special Publication 23, p. 709–734.
- Turner, S.J., Reynolds, G., and Hagemann, S.G., 2020, Boddington: An enigmatic giant Archean gold-copper (molybdenum-silver) deposit in the southwest Yilgarn craton, Western Australia: Society of Economic Geologists, Special Publication 23, p. 275–288.
- Walker, T.L., 1930, Dalmatianite, the spotted greenstone from the Amulet mine, Noranda, Québec: University of Toronto Studies, Geological Series No. 29: Contributions to Canadian Mineralogy, 1930, p. 9–12.
- Watkins, D.H., and Riverin, G., 1982, Geology of the Opemiska copper-gold deposits at Chapais, Quebec: Geological Association of Canada, Special Paper 25, p. 427–446.
- Wilkinson, L., Cruden, A.R., and Krogh, T.E., 1999, Timing and kinematics of post-Timiskaming deformation within the Larder Lake-Cadillac deformation zone, southwest Abitibi greenstone belt, Ontario, Canada: Canadian Journal of Earth Sciences, v. 36, p. 627–647.
- Wilson, M.E., 1941, Noranda district, Québec: Geological Survey of Canada, Memoir 229, 162 p.
- ——1956, Early Precambrian rocks of the Timiskaming region, Quebec and Ontario, Canada: Geological Society of America Bulletin, v. 67, p. 1397–1430
- Zubowski, S., 2011, Characterization of hydrothermal fluids within synvolcanic faults of the ~2.7 Ga, mine sequence, Noranda District, Québec: M.Sc. thesis, Sudbury, Ontario, Laurentian University, 168 p.

Marina Schofield received her Ph.D. degree from the Harquail School of Earth Sciences at Laurentian University in Sudbury, Canada. Her research focused on the metallogeny of the Powell block, Rouyn-Noranda, Quebec with an emphasis on field mapping. She has a strong background in volcanology, structural geology and base and precious metal



deposits. She received her B.Sc. in earth sciences from Memorial University of Newfoundland, Canada, and her M.Sc. in earth sciences from The University of Auckland, New Zealand. She has a keen interest in mineral exploration and is currently working as a project geologist for the Geological Survey of Newfoundland and Labrador, Mineral Deposits Division.

